Theses and Dissertations   1. Thesis and Dissertation Collection, all items

1996-03

Simulation of an optical correlator configured as an imaging system using liquid crystal television spatial light modulators

Miller, Scot C.

Monterey, California. Naval Postgraduate School

http://hdl.handle.net/10945/32187

NAVAL POSTGRADUATE SCHOOL
Monterey, California

THESIS

SIMULATION OF AN OPTICAL CORRELATOR
CONFIGURED AS AN IMAGING SYSTEM USING LIQUID
CRYSTAL TELEVISION SPATIAL LIGHT MODULATORS
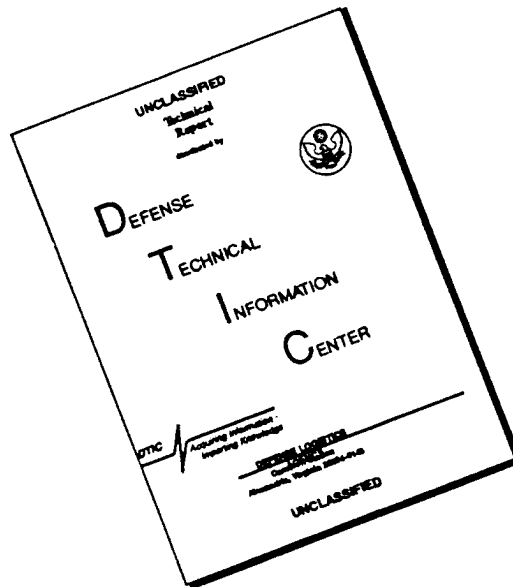
by

Scot C. Miller

March 1996

Thesis Advisor: John P. Powers

Approved for public release; distribution is unlimited.

19960508 141

DISCLAIMER NOTICE

1. AGENCY USE ONLY *(Leave blank)*	2. REPORT DATE 1 March 1996.	3. REPORT TYPE AND DATES COVERED Master's Thesis
4. TITLE AND SUBTITLE SIMULATION OF AN OPTICAL CORRELATOR CONFIGURED AS AN IMAGING SYSTEM USING LIQUID CRYSTAL TELEVISION SPATIAL LIGHT MODULATORS		5. FUNDING NUMBERS
6. AUTHOR(S) Scot Charles Miller		
7. PERFORMING ORGANIZATION NAME(S) AND ADDRESS(ES) Naval Postgraduate School Monterey CA 93943-5000		8. PERFORMING ORGANIZATION REPORT NUMBER
9. SPONSORING/MONITORING AGENCY NAME(S) AND ADDRESS(ES)		10. SPONSORING/MONITORING AGENCY REPORT NUMBER

11. SUPPLEMENTARY NOTES The views expressed in this thesis are those of the author and do not reflect the official policy or position of the Department of Defense or the U.S. Government.

12a. DISTRIBUTION/AVAILABILITY STATEMENT Approved for public release; distribution is unlimited.	12b. DISTRIBUTION CODE

13. ABSTRACT *(maximum 200 words)*

This thesis models the complex transmittance effects of liquid crystal television spatial light modulators (SLMs) in an optical correlator configured as an imaging system. The computer model implements both the ideal transmittance and the nonlinear measured transmittance which is a function of the voltage applied across the pixel of the liquid crystal device. The system modeled included the effects of a nonlinear input SLM input but assumed an ideal filter SLM. Input waveforms included both one-dimensional and two-dimensional spatial cosines and chirped cosines. Results show that the effects of the SLM transmittance nonlinearity can be minimized by limiting the input signal voltages to values falling on a piecewise linear region of the transmittance operating characteristics.

14. SUBJECT TERMS Optical Correlator; Spatial Light Modulator; Liquid Crystal Television Cell.			15. NUMBER OF PAGES 91
			16. PRICE CODE

17. SECURITY CLASSIFICATION OF REPORT Unclassified	18. SECURITY CLASSIFICATION OF THIS PAGE Unclassified	19. SECURITY CLASSIFICATION OF ABSTRACT Unclassified	20. LIMITATION OF ABSTRACT UL

SIMULATION OF AN OPTICAL CORRELATOR CONFIGURED AS AN IMAGING SYSTEM USING LIQUID CRYSTAL TELEVISION SPATIAL LIGHT MODULATORS

Scot C. Miller

Major, United States Army

B.S., New Mexico State University

Submitted in partial fulfillment

of the requirements for the degree of

MASTER OF SCIENCE IN ELECTRICAL ENGINEERING

from the

NAVAL POSTGRADUATE SCHOOL

March 1996

Author: _____

Scot C. Miller

Approved by: _____

John P. Powers, Thesis Advisor

_____

Ron J. Pieper, Second Reader

_____

Herschel H. Loomis, Chairman

Department of Electrical and Computer Engineering

ABSTRACT

This thesis models the complex transmittance effects of liquid crystal television spatial light modulators (SLMs) in an optical correlator configured as an imaging system. The computer model implements both the ideal transmittance and the nonlinear measured transmittance which is a function of the voltage applied across the pixel of the liquid crystal device. The system modeled included the effects of a nonlinear input SLM input but assumed an ideal filter SLM. Input waveforms included both one-dimensional and two-dimensional spatial cosines and chirped cosines. Results show that the effects of the SLM transmittance nonlinearity can be minimized by limiting the input signal voltages to values falling on a piecewise linear region of the transmittance operating characteristics.

TABLE OF CONTENTS

ACKNOWLEDGEMENTS

My sincere thanks to Professor John Powers for his support, guidance and patience throughout the course of this endeavor. His willingness to assist me in an unknown undertaking and the insight he provided made this a meaningful experience.

My gratitude to Dr. Richard Juday of the Johnson Space Center Hybrid Vision Section for his initiative in providing the initial impetus for the thesis, for graciously furnishing lodging and work space during my sojourn to Houston, and for benefitting me with his considerable intellectual talents in the world of optical processing. His enthusiasm and affection for his project and his profession will continue to drive me in the pursuit of academic and technical proficiency.

My thanks also to Dr. Juday's staff at the Hybrid Vision Section for their superb moral and technical support during my time at JSC. Special thanks to Dr. Colin Soutar for providing his unique insight, unfailing expertise, and remarkable perseverance in his attempts to anoint the optically impure.

Finally, I would like to thank my wife Leslie for her unswerving and unconditional support during the duration of the thesis effort. For this, I shall be forever grateful.

I. INTRODUCTION

Optical correlators have the promise of reducing the computational time required in optical processing applications that require two-dimensional Fourier transforms (2D-FTs). This is because optical correlators take advantage of the natural property of spherical lenses to perform the 2D-FTs optically. An application that used a specially configured optical correlator as an imaging system was used in the development of this thesis. The configuration was implemented to study the properties of liquid crystal television (LCTV) cells for use in optical correlators. Optical correlators and optical correlation are discussed in detail in subsequent chapters.

The Hybrid Vision Section at the Johnson Space Center (JSC) is currently conducting research on real-time optical correlation with the goal of developing a tracking optical correlator for use in such space applications as autonomous docking and landing. The system will ultimately be able to identify a specific object (or feature) and to determine the azimuth, elevation, range, roll, pitch, and yaw of the object. The correlator that JSC is currently working on is hybrid in nature in the sense that it combines both optical and digital processing of image data to determine object identification and orientation. Input image data and the desired filter characteristics are transferred to liquid crystal television (LCTV) spatial light modulators (SLMs) by a digital computer; the correlation operation is performed by optical means [Ref. 1].

The nonlinear characteristics of spatial light modulators and the effect of these characteristics on the performance of optical correlators is not yet fully understood. The transmittance of a pixel of a SLM depends on the voltage applied to the pixel. Ideally, the transmittance is a linear function of the applied voltage; in practice, however, the transmittance is a nonlinear, complex function of the voltage applied to a pixel of the SLM. This complex transmittance affects not only the amplitude of the coherent wave being modulated, but also the phase of this wave. The goal of this thesis was to provide a means for examining the effects of an experimentally obtained transmittance curve for a given LCTV SLM on a known test signal using MATLAB, a commercially available computation software package, to simulate the optical correlator. The JSC correlator was configured to operate as an imaging system (as described later) and this system was modeled by computer simulation to provide a visual method for comparing the effects using simulated images with those obtained in the actual imaging system.

Chapter II provides an overview of the optical correlation process. It also describes a generic optical correlator, the 4f (i.e., 4 focal length) VanderLugt correlator, and then, specifically, the Johnson Space Center's Hybrid Vision Lab optical correlator, a modified 2f correlator. This chapter also provides a description of the types of spatial light modulators being used for these applications and their function. It concludes with a brief discussion of the characteristics of the LCTV SLMs under investigation by the Hybrid Vision Lab and some specifics of their application in the JSC optical correlator.

Chapter III delves into a more thorough treatment of liquid crystal television spatial light modulators and discusses the specific techniques used at the Hybrid Vision Lab to characterize the LCTV SLMs in their optical correlator. A comparison of two methods used to characterize the LCTV SLMs (implementation of a Mach-Zehnder interferometer and use of a novel method devised by Soutar of the Hybrid Vision Lab) is presented, as are the merits of choosing the second method over the first for characterizing the liquid crystal cells. Finally, the chapter concludes by giving the results of the characterization and illustrating the nonlinear transmittance of the SLMs, using plots of the transmittance phase and amplitude as a function of the full range of voltages that wereapplied to a given pixel.

Chapter IV describes the simulation program developed for this thesis and the results of its implementation using the SLM characterization data obtained in Chapter III. It details the development of the imaging model used in the simulation, discusses how the experimentally obtained SLM data was incorporated into the simulation, and compares images obtained from the simulation output with images from the actual imaging system. The signal used as an input to the system, a spatial chirp, is developed and one-dimensional images are created and used to simulate operation of the system using MATLAB and Spyglass transform, two software packages. The extension to two-dimensions follows and a comparison is made to the performance of the actual system. Additionally, a comparison of an "ideal" SLM, i.e., one with linear transmittance, is made with that of the transmittance from the actual SLMs used in the Hybrid Vision Lab

correlator to illustrate the effects of this nonlinear behavior on the performance of the imaging system. This chapter also looks at controlling the nonlinear effects of the SLMs by limiting the range of voltages being applied to each of the pixels.

Chapter V provides a summary of the results in the thesis and discusses possibilities for future thesis study. The Appendix gives the source code used for the simulation.

II. BACKGROUND

A. SPATIAL LIGHT MODULATORS

1. Description

Spatial light modulators are classified by the way they modify light. Several classes are possible depending on the complex amplitude transmittance, T, of the device, where T is of the form

$$T(v(x,y)) = \sqrt{I(v(x,y))} \exp(j\phi(v(x,y))). \tag{1}$$

Here, I is the fraction of the incident intensity that is transmitted, ϕ is the added phase of the transmitted light, and $v(x,y)$ is the voltage applied to the modulator at position (x,y). Rather than using x,y (the pixel position), we prefer to m,n to represent the pixel number (where m,n are integers). For a pixel located at position (m,n), the transmittance is of the form

$$T(v(m,n)) = \sqrt{I(v(m,n))} \exp(j\phi(v(m,n))), \tag{2}$$

where $v(m,n)$ is the voltage applied to the pixel at (m,n).

"Amplitude-only" SLMs are those where the amplitude of the transmittance changes as a function of applied voltage, but the phase remains constant [Ref. 5]. When T is plotted in the complex plane with $v(m,n)$ as a parameter, the plot is a straight line passing through the origin as shown on the left side of Figure 1. Similarly, "phase-only" SLMs affect only

5

the phase of the transmitted light but have no effect on the amplitude. When their transmittance is plotted in the complex plane as a function of applied voltage, they have a constant magnitude but a changing phase as shown on the right side of Figure 1. "Coupled" modulators are SLMs that have transmittance values that fall on a curve that is neither straight, nor a circular arc, nor does it pass through the origin. For these modulators, the values of *both* $\sqrt{I}$ and ϕ change as a function of the applied voltage. Finally, "discrete" modulators are complex SLMs that have their transmittance values drawn from a finite set of possible values; they are a special case of a coupled modulator. Figure 2 provides examples of curves for coupled and discrete modulators.
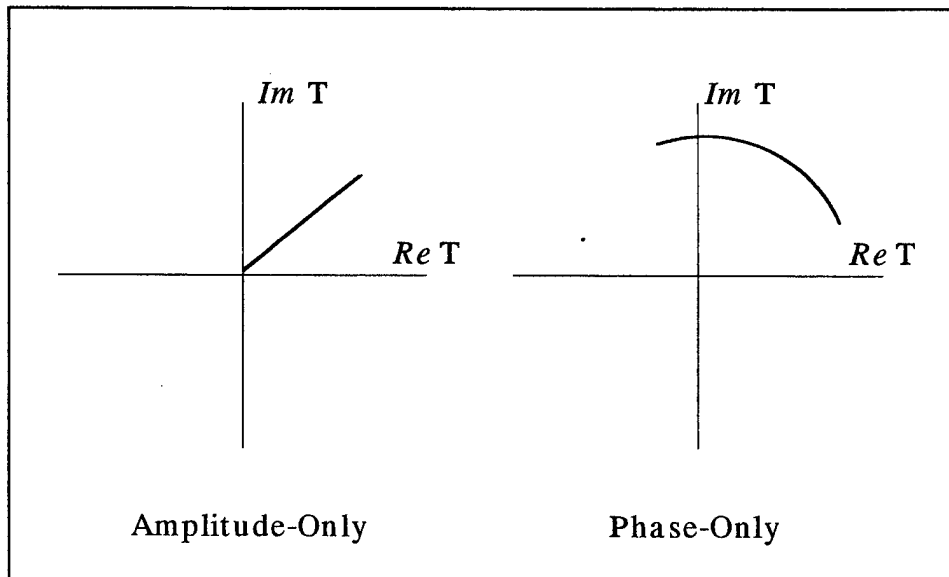
Figure 1. Left curve depicts amplitude-only SLM and right curve depicts phase-only SLM.

The liquid crystal cells used for this simulation are discrete modulators due to the quantized voltage levels applied to the pixel [Ref. 5].
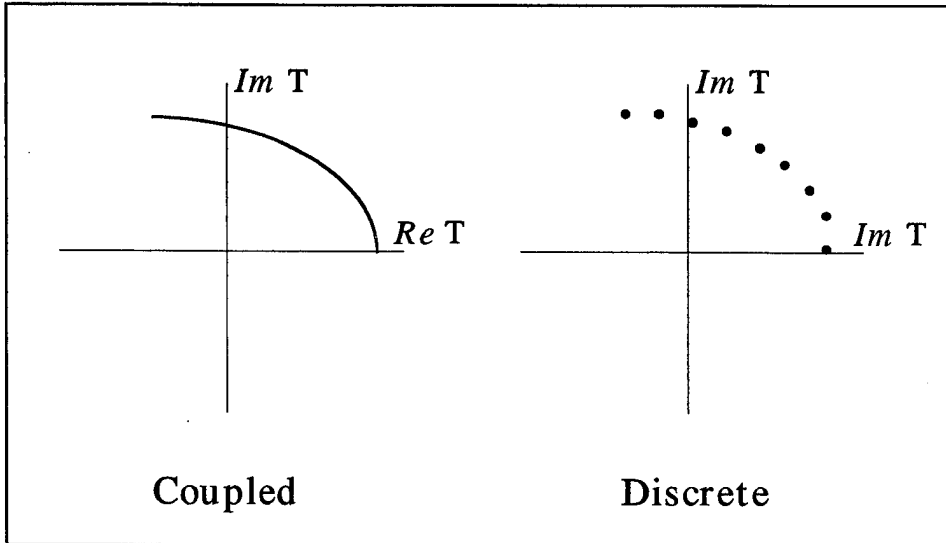
Figure 2. Left curve depicts coupled SLM and right curve depicts discrete SLM.

2. LCTV SLMs

The Hybrid Vision Lab optical correlator was constructed using two of the three liquid cells from a commercially available liquid crystal television (LCTV) projector, the Epson Crystal Image Video Projector (Model E1020) [Ref. 4]. The cells corresponding to the green and red video inputs on the LCTV were used for the input and filter plane modulators of the optical correlator, respectively. The separate RGB video inputs of the projector allow independent control of the drive signals to each of the cells.

The liquid crystal cells that were characterized for the simulation were of the twisted nematic type mounted between orthogonal linear polarizers. This type of liquid crystal is

7

anisotropic and has associated with it a molecular "director". The director refers to the alignment of the molecular structure of the crystal and is parallel to the optical axis of the crystal. Measurements have determined that the director of the SLMs rotates through approximately 80-90 degrees across the thickness of the cell, hence the liquid crystal is called "twisted" [Refs. 4 and 7].

The following discussion regarding the modulation characteristics of the Epson LCTV cells follows Ref. 4. The type of modulation achieved by the LCTV cell is dependent on the input and output polarizer settings and on the pixel's bias voltage $v(m,n)$. For normal operation of the projection TV, the input linear polarizer axis is set at 90 degrees relative to the director in the front of the cell. For the condition where no voltage is applied to the cell, the output light is also linearly polarized, but is rotated relative to the input. For an LCTV cell with a twist angle of 90 degrees, Cotariu et al. found that when the output polarizer is aligned at 90 degrees relative to the input polarizer, the light output is a maximum with 0 volts input to the cell [Ref. 4]. If the voltage to the cell is increased, the alignment of the linearly polarized output light from the liquid crystal is changed by an angle, θ, and the output light amplitude from the analyzer is decreased by the $\cos(\theta)$. For this mode, the phase shift of the light is usually small, and the modulation is considered "amplitude-mostly".

If the input polarizer is set such that its axis is parallel to the director in the front of the cell, and if the bias voltage applied to the cell is set to minimum, the output light amplitude from the analyzer varies little as the voltage to the cell is increased, and the

8

ouput phase varies as the voltage to the cell is increased. This type of modulation is referred to as "phase-mostly" operation. Phase modulation exceeding 360 degrees has been obtained using this configuration [Refs. 4 and 9]. Whereas amplitude and phase-only SLMs, as described in the previous subsection, are ideal cases, the amplitude and phase-mostly configurations described above are the best that can be achieved using actual LCTV SLMs.

Several groups [Refs. 4, 7, and 9] have reported that LCTV cells naturally exhibit a "coupled" behavior, as defined in subsection II.A.1, with respect to their modulation characteristics (i.e., both the phase and amplitude of the output light from the analyzer vary as voltage to the cell is varied). The LCTV SLM used in this thesis was characterized to show this coupled modulation behavior. The process used to characterize the SLM is described in detail in Chapter III.

B.   OPTICAL CORRELATION

The following discussion of optical correlation follows Ref. 3. The cross-correlation $c_{fg}(\tau_x, \tau_y)$ of two images $f(x,y)$ and $g(x,y)$ is given as:

$$
\begin{aligned}
c_{fg}(\tau_x,\tau_y) &= f(x,y) \otimes g(x,y) \\
&\equiv \int_{-\infty}^{\infty}\int_{-\infty}^{\infty} f(x,y)g(x+\tau_x,y+\tau_y)\, dx\, dy.
\end{aligned}
\tag{3}
$$

In this equation, $g(x,y)$ is the reference or target image that is being searched for in the scene $f(x,y)$. In general, f and g are complex. The cross-correlation will have large values at (τ_x, τ_y) combinations that correspond to the locations of $g(x,y)$ within $f(x,y)$ and small

values everywhere else. Therefore, if $c_{fg}(\tau_x, \tau_y)$ can be formed and searched for large

values, the presence of $g(x,y)$ in scene $f(x,y)$ can be detected and located. The two-

dimensional cross-correlation may be expressed in terms of spatial Fourier transforms as:

$$c_{fg}(\tau_x, \tau_y) = FT^{-1}\{F(u,v)G^*(u,v)\},\tag{4}$$

where FT^{-1} is the inverse two-dimensional Fourier transform and $F(u,v)$ is the two-

dimensional spatial Fourier transform of $f(x,y)$:

$$F(u,v) = \int\limits_{-\infty}^{\infty}\int\limits_{-\infty}^{\infty} f(x,y)e^{-j2\pi(ux+vy)}\,dx\,dy,\tag{5}$$

where u and v are the spatial frequencies. Likewise, $G(u,v)$ is the two-dimensional Fourier

transform of $g(x,y)$ and $G^*(u,v)$ is the complex conjugate of $G(u,v)$ [Ref. 3].

Typical imaging systems use optics at the front end of a system to gather the scene

and then process the information digitally. Computationally, the cross-correlation operation

of Equation 4 requires taking a 2D-FT of the input image $f(x,y)$, multiplying that by the

appropriate filter $G^*(u,v)$, and taking an inverse two-dimensional Fourier transform to

obtain the cross-correlation of the two.

Figure 3 shows the basic concept of a frequency plane correlator. The image $f(x,y)$

is realized by an SLM in the input plane, P1, and transformed optically by lens L1 with

the transform appearing in the filter plane, P2. When the input image, in the front focal

plane of lens L1, is illuminated by a coherent plane wave, the 2D-FT of $f(x,y)$ (i.e.,

10

$F(u,v)$) illuminates the filter SLM, P2, in the back focal plane of lens L1, which has the complex transmittance $G^*(u,v)$. A number of filters, representing the complex conjugates of the Fourier transforms of potential input scenes, are stored in the correlator's memory for use as inputs to the SLM located in the filter plane, P2. The light leaving the filter plane SLM is given by the product $F(u,v)G^*(u,v)$. A second 2D-FT is then realized in the correlation plane, P3, by passing this light through the second lens, L2. The second 2D-FT results in the cross-correlation of $f(x,y)$ and $g(x,y)$, except that optically, the effect of taking two successive forward 2D-FTs is a reversal of the coordinate axes in the correlation plane. Therefore, to achieve the desired result of Equation 4, the image in the correlation plane must be reversed (either electronically or optically) [Ref. 3]. When the Fourier transform of the input scene matches the selected filter exactly, the correlation peak at the output of the correlator manifests itself as a bright spot in the the correlation plane, P3. The position of the spot corresponds to the position of the image in the input plane. The intensity of the spot in the correlation plane provides a measure of the strength of the match (i.e., the brighter the spot, the better the match) [Ref. 8].

Frequency Plane Correlator

INPUT   FILTER   CORRELATION

P1   L1   P2   L2   P3
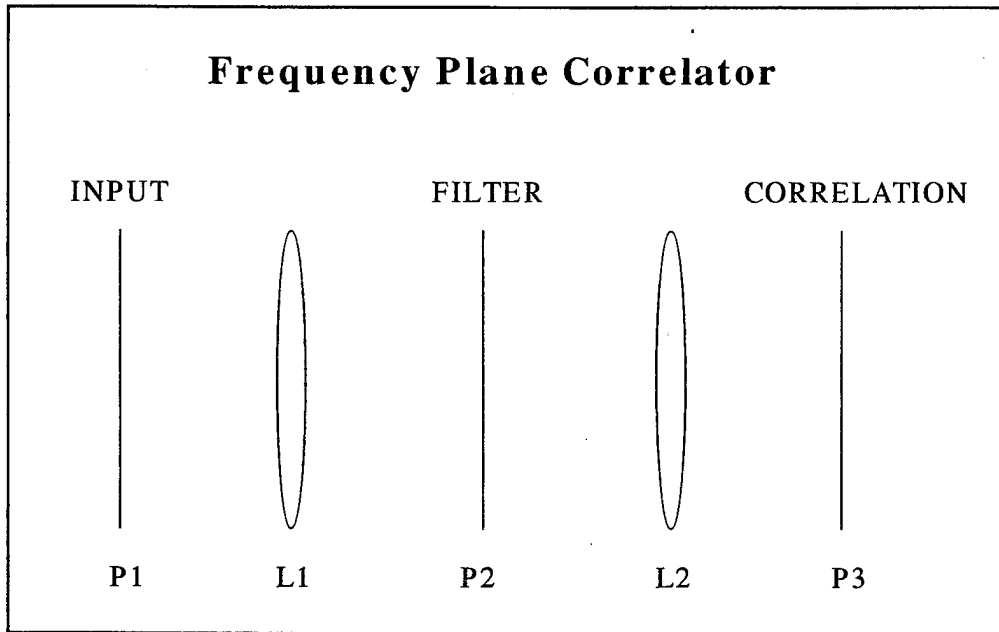
Figure 3. Schematic of a Frequency Plane Correlator.

In applications such as autonomous docking of spacecraft or other scene recognition scenarios, the input scene is an arbitrary image; therefore several filters might be required before the desired correlation peak is obtained. As mentioned above, the filters are complex conjugates of the Fourier transforms of potential input scenes (i.e., for the autonomous docking application, these might be several orientations of a spacecraft). The filters are transferred to the filter plane at a fixed rate and the correlation plane evaluated prior to the selection of the next filter. A substantial computational savings may therefore be realized by the use of optical means to perform the correlation operation rather than using digital processing methods since there is a finite processing time associated with the latter. The next two sections provide a description of a generic optical correlator, the 4f

VanderLugt correlator, and then describe the modified 2f correlator implemented by the JSC Hybrid Vision Section.

1. 4f Correlator

Figure 4 shows the block diagram for the 4f VanderLugt correlator [Ref. 2]. The focus lens, light pinhole and collimating lens are a beam expander that produces an approximate plane wave at the *input plane* (i.e., the location of SLM1). We will assume that this plane wave has an amplitude A and a phase of zero so that the phasor representation of the plane wave at the input side of the input plane is

$$\tilde{L}_{i\ input} = Ae^{j0} = A. \tag{6}$$

(In using phasor notation, we can convert the phasor to the wave by performing the operation

$$l(x,y,z,t) = Re\{\tilde{L}e^{j2\pi(vt-(z/\lambda))}\} \tag{7}$$

where the wave is traveling in the $+z$ direction.)

13

4f VanderLugt Correlator

$$\vdash\!\!-\!f_1\!-\!\!-\!\!\dashv\!\!-\!f_1\!-\!\!-\!\dashv\!\!-\!f_2\!-\!\dashv\!\!-\!f_2\!-\!\dashv$$

Laser Collimating FTL1   FTL2
    Lens

Focus Pinhole Input   Filter   Correlation
Lens   Plane   Plane   Plane
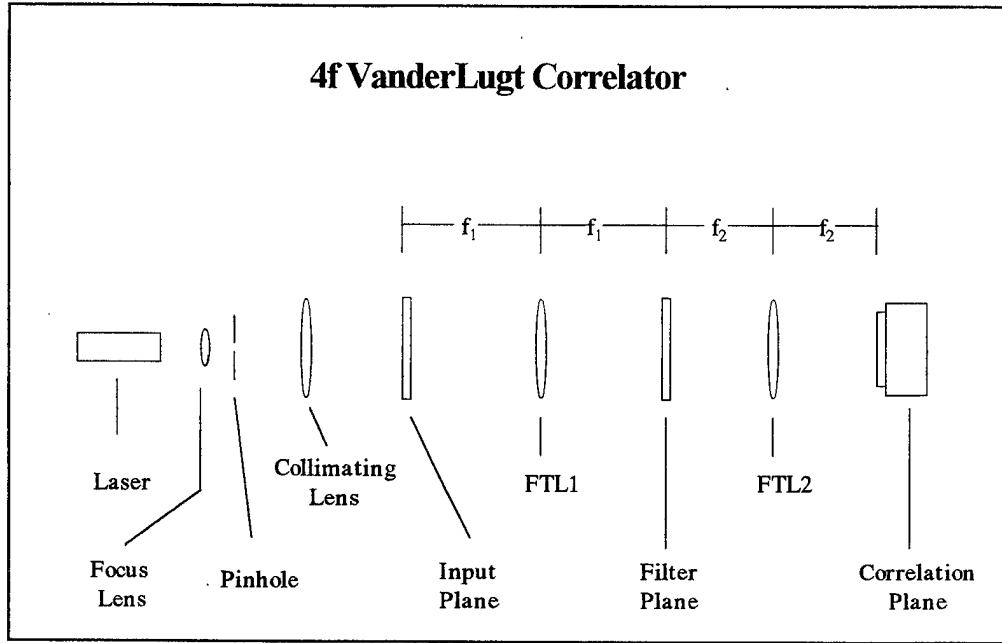
Figure 4. 4f VanderLugt Optical Correlator. (From Ref. 2.)

The scene $f(x,y)$ is applied electronically to SLM1 under computer control; the transmittance of SLM1, T_1, is (ideally) linearly proportional to $f(x,y)$,

$$T_1(x_{input}, y_{input}) = kf(x_{input}, y_{input}), \tag{8}$$

where k is a constant of proportionality. The output of SLM1 is the product of the input light wave and the transmittance,

$$\tilde{L}_{o\ input} = T_1 \tilde{L}_{i\ input} = kAf(x_{input}, y_{input}). \tag{9}$$

(Note that this is how we can achieve the multiplication operation in optics.)

14

One of the characteristics of a spherical lens operating with coherent light is that, if an arbitrary spatial light distribution is placed in the front focal plane of a lens (i.e., one focal length in front of this lens), then the light distribution in the back focal plane (one focal length behind the lens) is the two-dimensional Fourier transform of the input distribution [Ref. 10]. Thus, optics can easily compute the two-dimensional Fourier transform. We place the output of SLM1 in the front focal plane of a lens, FTL1, of focal length f_1 (as in Fig. 4) and the light distribution at the back focal plane (called the *filter plane*) will be

$$\tilde{L}_{i\,filter}(x_{filter}, y_{filter}) = \mathscr{F}\{\tilde{L}_{o\,input}\} = kAF(x_{filter}, y_{filter}) \tag{10}$$

where, for simplicity, we have ignored amplitude and size scaling constants.

In the back focal plane of this first transforming lens, we place a second spatial light modulator, SLM2. We then electronically apply a desired filter function G^* to the SLM under computer control. The transmittance of SLM2 is, again, proportional to G^*, so

$$T_2(x_{filter}, y_{filter}) = kG^*(x_{filter}, y_{filter}) \tag{11}$$

where we have assumed the same constant of proportionality, k, as SLM1. The light distribution at the output of SLM2 is the product of the light distribution (Eq. 10) and T_2,

$$\tilde{L}_{o\,filter}(x_{filter}, y_{filter}) = k^2 AF(x_{filter}, y_{filter})G^*(x_{filter}, y_{filter}). \tag{12}$$

15

We now should perform the inverse two-dimensional Fourier transform of this light distribution, but this operation is not easily done optically. Instead we recall that the transform of the transform of a function returns an inverted version of the function, i.e.,

$$\mathscr{F}\{\mathscr{F}\{f(x,y)\}\} = f(-x,-y). \tag{13}$$

Optically, two successive transforms will return an inverted version of the original light distribution. (As previously mentioned, inverted images are easily reversed electronically or optically in our display.) So, we place a second lens, FTL2, one focal length away from the output of SLM2. (See Fig. 4.) In the back focal plane of this lens (called the correlation plane), we will have the two-dimensional transform of the light out of SLM2 (Eq. 12), or

$$\tilde{L}_{correlation}(x_{correlation}, y_{correlation}) = k^2 A \mathscr{F}\{FG^*\}$$
$$= k^2 A c_{fg}(-x_{correlation}, -y_{correlation}). \tag{14}$$

Again, scaling constants in amplitude and size have been omitted for simplicity. A charge-coupled device (CCD) camera detects the intensity of the light in the correlation plane. This intensity pattern is displayed on a standard video output device with the cross-correlation peaks appearing as bright spots in the display. Axis reversal is compensated by manipulation of the intensity pattern using a control computer that is interfaced with the video output device. Hence, we see that the 4f correlator does, indeed, perform the two-dimensional cross-correlation operation. If the focal lengths of the two transforming lenses

16

are equal, the length of the optical system (without the beam expander) is four times the focal length.

LCTV SLMs can be used at the input and filter planes to place the input $f(x,y)$ and filter $G^*(x,y)$ images in the correlator. The transmittance of these LCTV SLMs is non-ideal; this is discussed in detail in Chapter III. The 4f system is an adequate correlation system with the exception of its length. For this reason, the system adopted by the JSC Hybrid Vision Lab is the modified 2f system.

2. Modified 2f Correlator

Figure 5 illustrates the modified 2f system implemented by the Hybrid Vision Section [Ref. 4]. The 2f system is attained by using the thin lens combination formula,

$$\frac{1}{f_{new}} = \frac{1}{f_{1\ old}} + \frac{1}{f_{2\ old}}, \tag{15}$$

to combine two contacting lenses (i.e., to calculate a new single, equivalent lens with focal length f_{new}) and to move the relative placement of the input and filter planes to reduce the required dimensions of the correlator. A brief description of the lens combination process as it applies to the 2f system of Figure 5 is given here; a thorough treatment of the subject is provided by Reference 2.
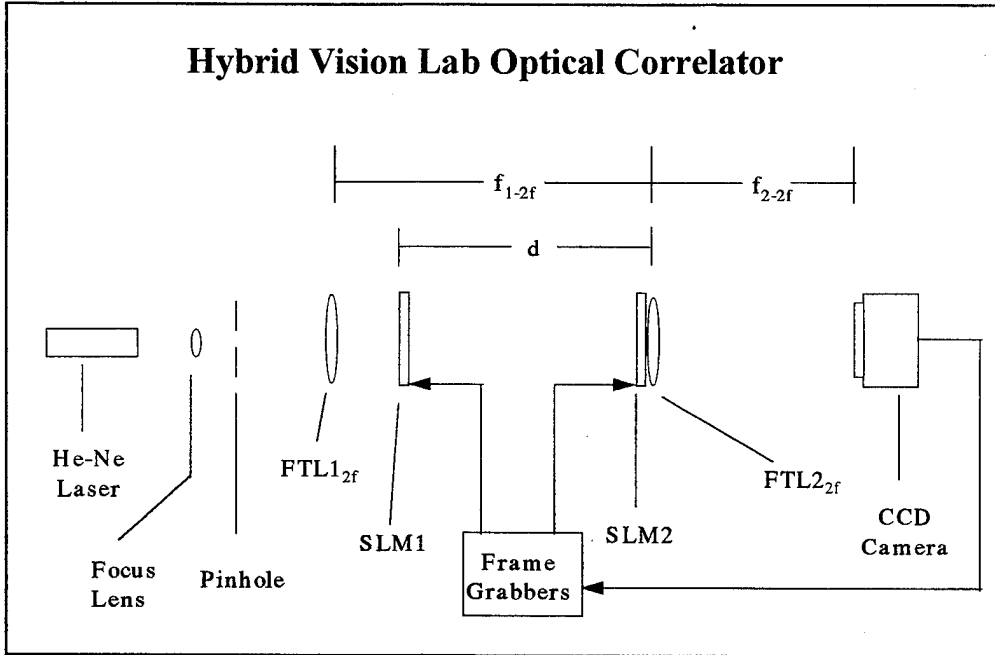
Hybrid Vision Lab Optical Correlator

Figure 5. Hybrid Vision Lab modified 2f optical correlator.

The input plane of the 4f correlator, consisting of the first liquid crystal spatial light modulator, SLM1, is moved behind the first Fourier transform lens. This introduces a quadratic phase factor at the filter plane that is proportional to the distance d between the input and filter planes as detailed in Chapter IV. A phase compensation lens with focal length equal to d is (conceptually) placed next to the filter SLM, SLM2, to eliminate this phase error. The second Fourier transform lens in the 4f correlator, FTL2, is moved to this phase compensation lens and combined, according to Equation 15, to form the second lens in the 2f correlator, FTL2$_{2f}$. The focal length of this lens is $f_{2\text{-}2f}$ and is calculated using the thin lens formula, $1/f_{2\text{-}2f} = 1/d + 1/f_2$. Although this combination introduces a second quadratic phase factor in the light distribution in the correlation plane (as discussed in Chapter IV), this phase is irrelevant since the correlation is intensity detected by the CCD

camera and all phase information is lost. Because the light after the first collimation lens in the 4f system is parallel, the entire system described above is moved toward the collimation lens until the first Fourier transform lens touches the collimation lens. Again using Equation 5, these two lenses are combined to form $FTL1_{2f}$ with focal length equal to f_{1-2f} [Ref. 2]. Correlation-plane signal-to-noise ratios for this implementation have been found to exceed 100:1 [Ref. 4].

The frame grabbers illustrated in Figure 5 (manufactured by Imaging Technology Inc.) are digital-to-analog (D/A) and analog-to-digital (A/D) devices that provide the interface between the correlator control computer and the input and filter SLMs. The frame grabbers are used to convert the digital output from the computer to a voltage for use by SLM1 and SLM2 and a third frame grabber digitizes the signals from the CCD camera for further manipulation by the correlator computer. This data may then be either displayed or analyzed as desired.

To provide an accurate simulation of the Hybrid Vision Lab correlator, the measured transmittance of the actual LCTV SLMs was desired. Although phase-mostly and amplitude-mostly configurations of polarization settings were achieved, the configuration chosen for the simulation was a coupled (as described in Subsection II.A.1), discrete configuration (i.e., equivalent to that shown in the right half of Figure 2). The next chapter details the method used to determine the associated transmittance of these SLMs.

III. SLM CHARACTERIZATION

The Hybrid Vision Lab correlator was set-up as described in Chapter II using the *green* and *red* liquid crystal cells from the Epson Model E1020 color TV projection unit for the input and filter plane SLMs. The setup was configured to obtain a maximum correlation peak using a known test pattern (i.e., using a known image at the input SLM of the correlator and the complex conjugate of the Fourier transform at the filter SLM); the correlator hardware was then positioned to obtain the maximum correlation peak possible. The complex transmittance curve was then determined for the input SLM for use in the simulation. The magnitude of the transmittance is measured fairly easily; the phase measurement is more difficult. We will begin with the phase response measurement.

A. BACKGROUND

The standard method for measuring a phase shift in a transmissive device is the use of interferometric techniques. One of the methods for measuring the SLM's phase shift as a function of applied voltage involves implementation of a Mach-Zehnder interferometer. Figure 6 shows the generic set-up for this type of interferometer. A monochromatic, plane-wave laser beam passes through a beam splitter. In the lower arm of the interferometer, the beam passes through the liquid crystal cell and lens L_2 Fourier transforms the output light from the LCTV. The input beam splitter, mirror M_1, and output beam splitter produce a slightly tilted plane wave at plane P_2. The final beam splitter allows recombination of the waves that are displayed as interference fringes on an intensity-

sensitive detector, in this case an electronic imaging device, at P_2. A computer is connected to the liquid crystal cell which allows the voltage applied to the pixels of the cell to be increased in 256 discrete steps. Each of the discrete steps represents a unique value of gray-scale. As the voltage applied to all pixels of the liquid crystal cell is incrementally stepped from that corresponding to 0 gray-scale to the voltage corresponding to 255 gray-scale, the relative movement of the fringes provides a measure of the relative phase shift of the transmittance as a function of the gray-scale.
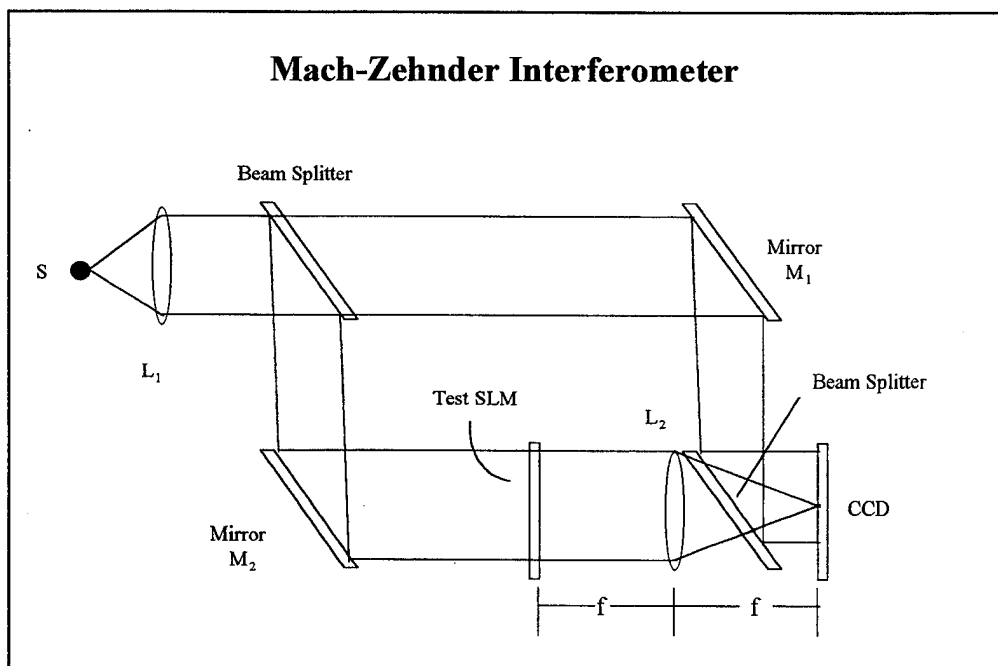

Figure 6. Modified Mach-Zehnder Interferometer. (After Ref. 7).

A method that proved to be more suitable to the task of characterizing the liquid crystal cells, especially for the phase shift measurement, was that devised by Soutar at the

Hybrid Vision Lab of the Johnson Space Center [Ref. 9]. The laboratory set-up for this method is shown at Figure 7. This set-up was chosen over the Mach-Zehnder interferometer because the the fringes were more stable. This is because the two beams forming the interference pattern pass through the same optical components and are therefore subject to the same mechanical movements. For characterization of the LCTV cells, this translated into improved measurement of the relative translation of the two beams.
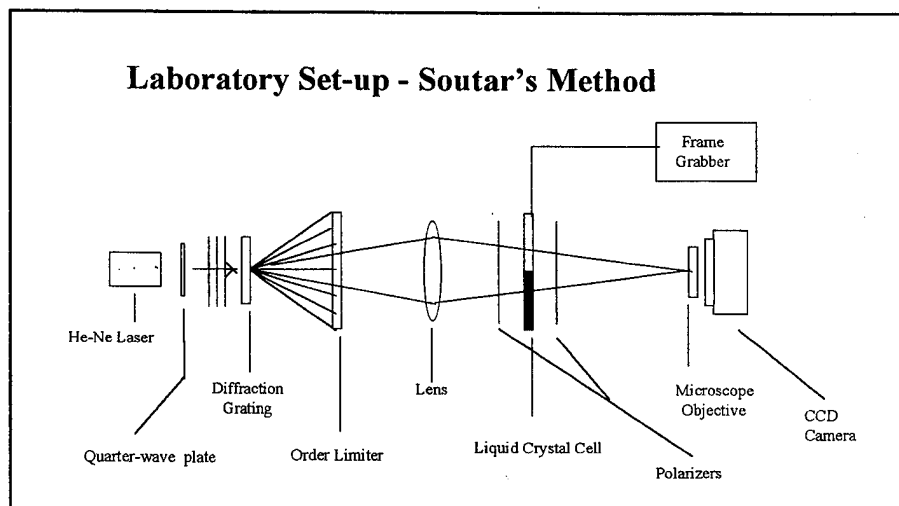

Figure 7. Laboratory set-up for characterization of liquid crystal cell using Soutar's method. (After Ref. 9).

The input to the system is a monochromatic plane wave. This passes through a Ronchi-ruling diffraction grating which splits the light into several diffraction orders. These encounter an order limiter, a piece of cardboard that acts as a crude spatial filter and blocks all but the two first-order beams. These two beams pass through a lens and are focused toward the liquid crystal cell.

23

For the phase characterization, the frame grabber places a different video pattern on each half of the LCTV cell. On one-half of the cell, this pattern is kept at a constant level equivalent to a gray-scale value of 0 (i.e., the pixels on one-half of the cell are addressed with the voltage corresponding to 0 gray-scale). On the other half of the cell, the pattern is sequentially incremented in gray-scale steps of 10 from a value corresponding to 0 gray-scale up to the value corresponding to 250 gray-scale, plus an additional value corresponding to gray-scale 255. One of the diffraction orders passes through the region of fixed gray-scale and the other passes through the region of varying gray-scale. Each of the beams passes through a circular area with a 24-pixel diameter, which, for the two beams, represents approximately 1.3 percent of the total LCTV SLM pixels [Ref. 9]. A conceptual representation (head-on view) of this arrangement is shown at Figure 8. The two orders focus on a microscope objective (Fig. 7) where they recombine to form a fringe pattern that is magnified onto a CCD camera. For the measurements, as the frame-grabber steps the one gray-scale pattern through the full range of values as described (i.e., values of 0, 10, 20, 30, ..., 250, and 255), a second frame-grabber grabs a single line of the output (i.e., a single row of pixels) from the CCD camera for each of the increments of gray-scale. The relative phase shift caused by the different video signals on the two halves of the SLM is obtained by observing the fringe translation.

Soutar used an image processing program, ASYST, to analyze the collected fringe data. Using a least squares method, the program found the minima of the fringes, determined the fringe shift, and calculated the relative shift, in radians. A plot of this

24

relative phase shift as a function of applied gray-scale value provides the phase of the transmittance of the SLM.

Liquid Crystal Cell

1st-order
diffraction
beams

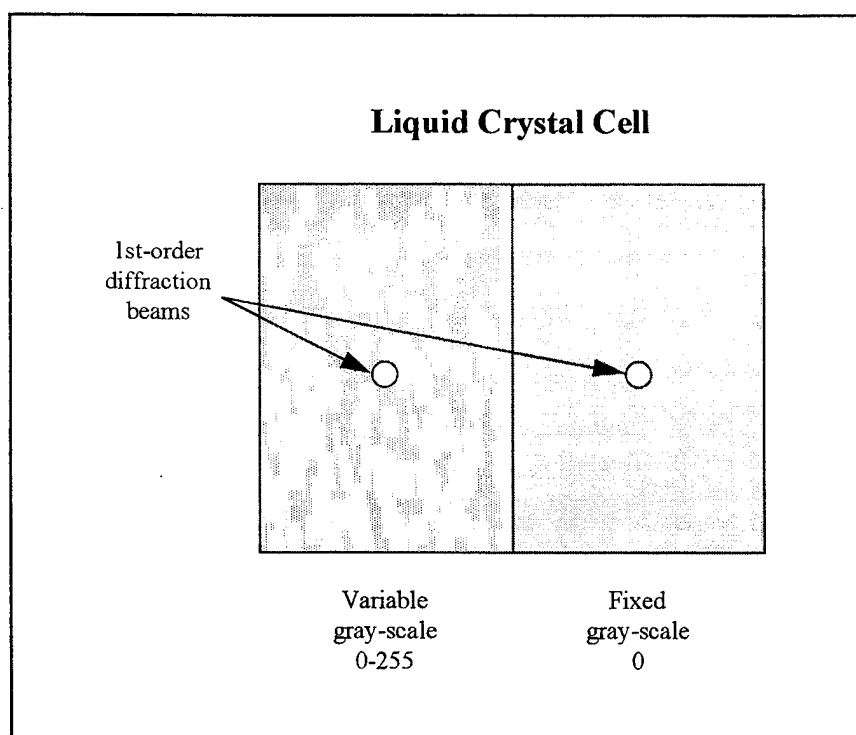Variable
gray-scale
0-255

Fixed
gray-scale
0

Figure 8. Illustration of liquid crystal cell phase characterization technique.

Amplitude characterization of the cell requires blocking the first-order beam passing through the 0 level region and passing the remaining beam through the variable gray-scale half of the liquid crystal cell. As the frame grabber cycles the LCTV gray-scale values from 0 to 250 in steps of 10, an optical power meter in the back focal plane of the lens measured the corresponding intensity at each of the values. In addition, the intensity transmittance at the gray-scale value of 255 was recorded. The square-root of the intensity

transmittance at each of the applied-voltage values provides the amplitude transmittance for the SLM.

B. MEASUREMENT RESULTS

The two LCTV SLMs in the optical correlator were characterized in this fashion after the correlator was optimized to obtain a maximum correlation peak using a known test pattern. The input and output polarizer rotational settings for each of the liquid crystal cells and the brightness control on the LCTV base unit were preset for optimal correlator operation, and then the liquid crystal cells were characterized in-situ.

The values of intensity versus gray-scale and phase shift versus gray-scale obtained for the input modulator are given in Tables I and II, respectively. Figure 9 provides plots of these data.

TABLE I. Values for Intensity Transmission as a Function of Gray-scale for SLM1.

GRAY-SCALE	INTENS. (Norm.)	GRAY-SCALE	INTENS. (Norm.)	GRAY-SCALE	INTENS. (Norm.)
0	0.868	90	0.269	180	0.149
10	0.953	100	0.177	190	0.189
20	1.000	110	0.108	200	0.229
30	0.974	120	0.067	210	0.271
40	0.891	130	0.047	220	0.312
50	0.794	140	0.046	230	0.356
60	0.656	150	0.059	240	0.403
70	0.527	160	0.082	250	0.435
80	0.391	170	0.112	255	0.453

TABLE II. Values for Phase Shift in Radians as a Function of Gray-scale for SLM1.

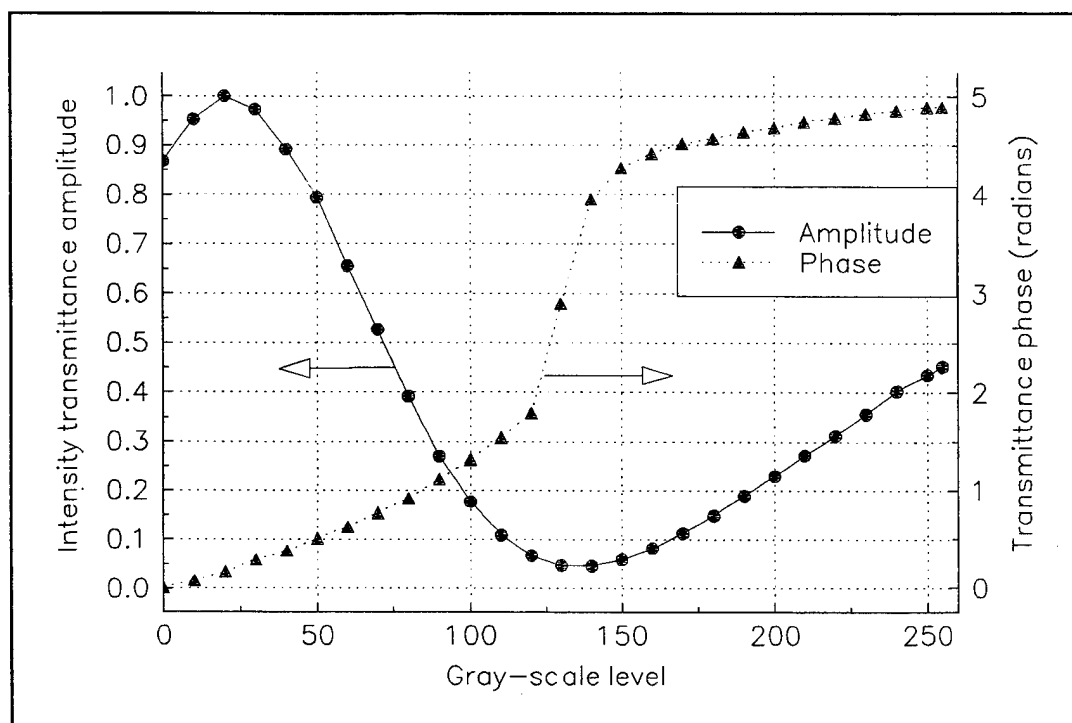| GRAY-SCALE	PHASE SHIFT	GRAY-SCALE	PHASE SHIFT	GRAY-SCALE	PHASE SHIFT
0	0.000	90	1.106	180	4.570
10	0.073	100	1.312	190	4.637
20	0.166	110	1.537	200	4.684
30	0.285	120	1.788	210	4.743
40	0.378	130	2.894	220	4.783
50	0.503	140	3.955	230	4.823
60	0.623	150	4.272	240	4.857
70	0.768	160	4.419	250	4.890
80	0.914	170	4.518	255	4.895

Figure 9. Measured intensity transmittance vs. pixel gray-scale level. The amplitude of the intensity transmittance (left axis) and phase shift (right axis) are plotted.

Figure 10 is a plot of the measured data in the complex plane. Noting the nonlinear nature of the transmittance curve and considering that it might have an adverse effect on a signal processed by the imaging system led to a requirement for a simulation program to provide the capability for the operator to select a piecewise-linear portion of the transmittance curve by choosing the corresponding gray-scale value associated with the desired range of the transmittance curve. Inspection of Figure 9 indicates that two portions of the normalized amplitude transmittance curve that are reasonably linear are those corresponding to 20-120 gray-scale and 140-250 gray-scale. Chapter IV, therefore,

discusses the modeling of the correlator for simulation with primary consideration of the
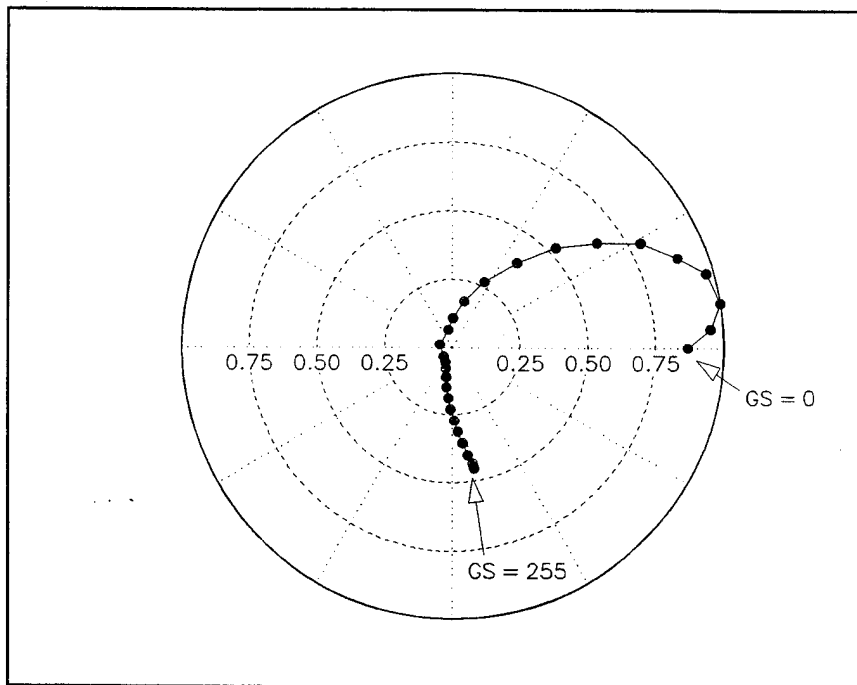
nonlinear aspect of the SLMs transmittance.

Figure 10. Plot of measured complex transmittance for SLM1 in the complex plane. Gray-scale values of end-points are noted.

IV. SIMULATION OF THE CORRELATOR AS AN IMAGING SYSTEM

Measurement of the transmittance characterization of the SLMs provided the necessary experimental data for input to the imaging system model. The particular correlator modelled in this thesis assumed an unaddressed filter SLM with unity amplitude transmittance (i.e., transmittance equal to $1e^{j0}$). Therefore, the resulting model is equivalent to a correlator configured as an (inverting) imaging system. This chapter details the development of the model for this system, discusses the incorporation of the measured and ideal SLM data into the simulation, and provides a comparison of the simulation results with those obtained from the actual system.

A. ASSUMPTIONS

The imaging system simulation developed for the thesis included the following assumptions. The system modelled was the modified 2f correlator discussed in Chapter II. The illumination was a uniform monochromatic plane wave. The input SLM was characterized from the data found using Soutar's method, discussed in Chapter III. The complex transmittance, as determined experimentally, was considered to be the same for each pixel in the SLM array. The filter-plane SLM was assumed to be "unaddressed" (i.e., the cell had only a bias voltage applied, essentially equivalent to the gray-scale level 20 shown in Fig. 9) for the purposes of simulation and subsequently for verification of the simulation; therefore, a unit-amplitude, constant-phase transmittance was assumed for the filter. Although this assumption was insignificant to the performance of the simulation of

31

the correlator as an imaging system, it would have a significant impact for the simulation of the correlator with an "addressed" filter plane SLM.

B. SPATIAL CHIRP EXCITATION

1. Desired Characteristics

Several candidates for an appropriate spatial signal for the SLM were studied for their relative desirability as an input to the system. Desirability in this sense meant finding a signal with a broad spatial frequency content so that its energy would be spread across the entire filter plane SLM. This specification will have utility in follow-on work for determining appropriate filters to use in standardizing correlator set-up.

2. Spatial Chirp Signal

With this criteria in mind, the signal chosen was the spatial chirp or linear FM signal. The goal was to provide a signal of the form

$$v(m,n) = C + A(m,n)\sin(\psi(m,n)), \tag{16}$$

where $v(m,n)$ is the desired spatial drive voltage signal, C is a constant, and $A(m,n)$ and $\psi(m,n)$ are the m-th horizontal and n-th vertical pixel's amplitude transmittance and phase shift. A one-dimensional SLM was modeled, i.e., a single row of pixels of length $N=256$. The implemented chirp equation mathematically is

$$v(m) = offset + gain\left\{\sin\left[m\left(f_o + \frac{f_d}{2}\right) - \left(\frac{f_d}{2} \cdot \frac{N-1}{2\pi}\right)\sin\left(\frac{2\pi m}{N-1}\right)\right]\right\}, \tag{17}$$

where f_o is the reference or carrier frequency, f_d is the maximum frequency deviation about f_o (both in radians), and m is the m-th pixel location. To allow the voltage to vary the magnitude of the transmittance over the full range of gray-scale values from 0 to 255, the amplitude, A, requires an *offset* value of 255/2 (or 127.5) and a *gain* value of 127.5. The computer simulation provides a means for selecting the maximum and minimum values of gray-scale available. The general forms for *offset* and *gain*, therefore, are that the *offset* equals one-half of the sum of the maximum and minimum gray-scale values selected, and the *gain* equals the *offset* minus the minimum gray-scale value selected. The resulting equation for the chirp function over the full range of gray-scale (0 to 255) is

$$v(m) = 127.5 + 127.5 \cdot \sin\left[m \left(f_o + \frac{f_d}{2} \right) - \left(\frac{f_d}{2} \cdot \frac{N-1}{2\pi} \right) \sin\left(\frac{2\pi m}{N-1} \right) \right]. \tag{18}$$

For comparison purposes, the simulation also provides for the selection of a cosine excitation that is given by

$$v(m) = offset + gain \left(\cos(m/10) \right). \tag{19}$$

The argument of the function was scaled by a factor of 10 to provide better resolution of this function, i.e., a fewer number of cycles.

C. CORRELATOR MODEL

The modified 2f correlator described in Chapter II was modeled in the following manner. A block diagram of the system is shown in Figure 11.
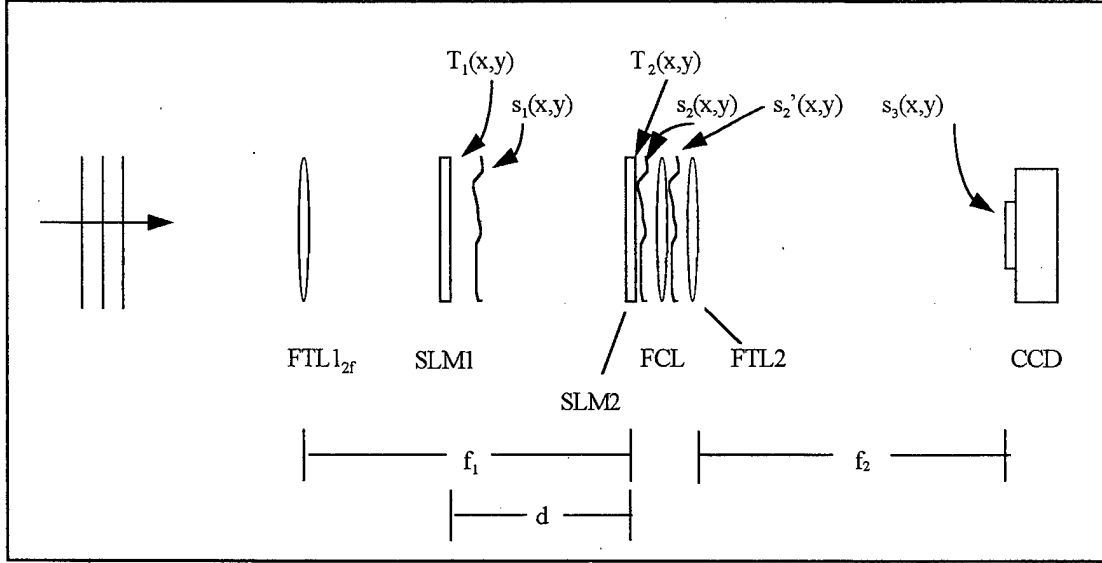

Figure 11. Model for 2f correlator including (conceptual) phase compensation lens, FCL, behind SLM2..

The illumination is considered to be a normally incident, monochromatic plane wave with amplitude, A. The light, $s_1(x,y)$, at the output spatial light modulator SLM1 is [Ref. 10]

$$s_1(x_1,y_1) = \frac{Af_1}{d} P\left(\frac{x_1f_1}{d}, \frac{y_1f_1}{d}\right) e^{\left(-j\frac{k}{2d}(x_1^2+y_1^2)\right)} T_1(x_1,y_1), \tag{20}$$

where the pupil function, $P(x,y)$, accounts for the finite extent of the lens aperture and has a value of 1 if SLM1 is fully illuminated, as we shall assume. The complex transmittance of SLM1 is represented by $T_1(x,y)$. Assuming that the filter SLM has a complex

34

transmittance $T_2(x,y)$, the light at the output of the second SLM (SLM2) located in the filter plane is [Ref. 10]

$$s_2(x_2,y_2) = \frac{Af_1 e^{\left(j\frac{k}{2d}(x_2^2+y_2^2)\right)}}{j\lambda d^2} \tilde{T}_1\left(\frac{x_2}{\lambda d}, \frac{y_2}{\lambda d}\right) T_2(x_2,y_2) \qquad (21)$$

where

$$\tilde{T}_1\left(\frac{x_2}{\lambda d}, \frac{y_2}{\lambda d}\right) = \int_{-\infty}^{\infty}\int_{-\infty}^{\infty} T_1(x,y) e^{\left\{-j2\pi\left[\left(\frac{x_2}{\lambda d}\right)x + \left(\frac{y_2}{\lambda d}\right)y\right]\right\}} dx\ dy. \qquad (22)$$

We note that the left hand side of Eqn. 22 is the spatial Fourier transform of $T_1(x,y)$ evaluated at the spatial frequencies $f_x = x_2/\lambda d$ and $f_y = y_2/\lambda d$. Using a (conceptual) phase compensation lens, FCL, with a focal length $f = d$ introduces a phase factor $exp\ [-jk/2d\ (x_2^2+y_2^2)]$ that cancels the phase term of s_2, resulting in [Ref. 10]

$$\begin{aligned} s_2'(x_2,y_2) &= \frac{Af_1 e^{\left(\frac{jk}{2d}(x_2^2+y_2^2)\right)}}{j\lambda d^2} e^{\left(-\frac{jk}{2d}(x_2^2+y_2^2)\right)} \tilde{T}_1\left(\frac{x_2}{\lambda d}, \frac{y_2}{\lambda d}\right) T_2(x_2,y_2) \\ &= \frac{Af_1}{j\lambda d^2} \tilde{T}_1\left(\frac{x_2}{\lambda d}, \frac{y_2}{\lambda d}\right) T_2(x_2,y_2)\ . \end{aligned} \qquad (23)$$

Finally, in the correlation plane located a distance $f = f_2$ behind lens, FTL2, the light field is [Ref. 10]

$$s_3(x_3,y_3) = \left[\frac{Af_1}{j\lambda d^2}\right]\left[\frac{e^{j\frac{k}{2f_2}(x_3^2+y_3^2)}}{j\lambda f_2}\right] \cdot \mathscr{F}'\left\{\tilde{T}_1\left(\frac{x}{\lambda d},\frac{y}{\lambda d}\right)T_2(x,y)\right\}, \tag{24}$$

where $\mathscr{F}'\{\bullet\}$ indicates the two-dimensional spatial Fourier transform evaluated at the spatial frequencies $f_x=x_3/\lambda f_2$ and $f_y=x_3/\lambda f_2$. Combining terms and assuming that T_2 equals unity, we have [Ref. 10]

$$s_3(x_3,y_3)=\left[-\frac{Af_1 e^{j\frac{k}{2f_2}(x_3^2+y_3^2)}}{\lambda^2 d^2 f_2}\right] \cdot \mathscr{F}'\left\{\tilde{T}_1\left(\frac{x}{\lambda d},\frac{y}{\lambda d}\right)\right\}, \tag{25}$$

Using the similarity theorem [Ref. 10]

$$\mathscr{F}\{f(ax,by)\} = \frac{1}{|ab|}F\left(\frac{f_x}{a},\frac{f_y}{b}\right), \tag{26}$$

where

$$f(ax,by) = \tilde{T}_1\left(\frac{x}{\lambda d},\frac{y}{\lambda d}\right) \quad ; \quad a=b=\frac{1}{\lambda d}, \tag{27}$$

36

we get

$$\mathscr{F}'\left\{\tilde{T}_1\left(\frac{x}{\lambda d},\frac{y}{\lambda d}\right)\right\}=\lambda^2 d^2\ \hat{T}_1(f_x\lambda d, f_y\lambda d),\tag{28}$$

where $\hat{T}_1=\mathscr{F}'\{\tilde{T}_1\}$. Evaluating this transform at $f_x=x_3/\lambda d$ and $f_y=y_3/\lambda d$, we get

$$\lambda^2 d^2\,\hat{T}_1\left(\frac{x_3\lambda d}{\lambda f_2},\frac{y_3\lambda d}{\lambda f_2}\right)\ =\ \lambda^2 d^2\,\hat{T}_1\left(\frac{x_3 d}{f_2},\frac{y_3 d}{f_2}\right).\tag{29}$$

Since $\hat{T}_1(x,y)=\mathscr{F}\{\mathscr{F}\{T_1(x,y)\}\}$, we can apply the inversion theorem, $\mathscr{F}\{\mathscr{F}\{f(x,y)\}\}=f(-x,-y)$ which yields

$$\mathscr{F}'\left\{\tilde{T}_1\left(\frac{x}{\lambda d},\frac{y}{\lambda d}\right)\right\}\ =\ \lambda^2 d^2\,T_1\left(-\frac{x_3 d}{f_2},-\frac{y_3 d}{f_2}\right).\tag{30}$$

Substituting this result back into Eqn. 25 results in

$$\begin{aligned}
s_3(x_3,y_3)\ &=\ \left[-\frac{A f_1 e^{\frac{jk}{2f_2}(x_3^2+y_3^2)}}{\lambda^2 d^2 f_2}\right]\cdot(\lambda^2 d^2)\,T_1\left(-\frac{x_3 d}{f_2},-\frac{y_3 d}{f_2}\right)\\[2mm]
&=\ \left[-\frac{A f_1 e^{\frac{jk}{2f_2}(x_3^2+y_3^2)}}{f_2}\right]\cdot T_1\left(-\frac{x_3 d}{f_2},-\frac{y_3 d}{f_2}\right).
\end{aligned}\tag{31}$$

37

The (conceptual) phase compensation lens, *FCL*, and the Fourier transform lens, *FTL2*, are combined using the lens formula (Eq. 15), $1/f_{2-2f} = 1/d + 1/f_2$, to form the second lens in the 2f correlator model, $FTL2_{2f}$. A block diagram of the 2f model incorporating this lens is shown in Figure 12.
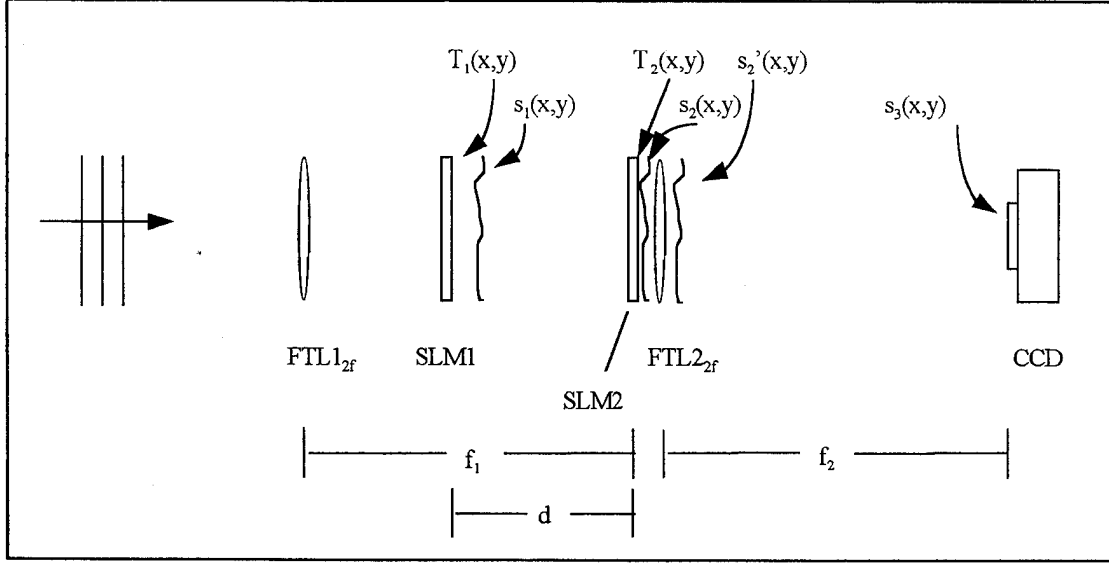

Figure 12. Final model for 2f correlator which includes the combination of the phase compensation lens, FCL, and the second Fourier transform lens, FTL2, into the equivalent lens, $FTL2_{2f}$.

A Charge Coupled Device (CCD) camera detects the intensity of the distribution in the correlation plane, giving

$$I_3(x_3,y_3) = |s_3(x_3,y_3)|^2$$
$$= \frac{A^2 f_1^2}{f_2^2} \left| T_1\left(-\frac{x_3 d}{f_2}, -\frac{y_3 d}{f_2}\right) \right|^2. \tag{32}$$

The correlator simulation calculates the output intensity as described in the preceding development using MATLAB to perform the operations [Ref. 10].

D. IMAGING SIMULATION

1. Introduction

The imaging simulation program was developed using two software packages, MATLAB and Spyglass Transform. MATLAB code was written to simulate the operation of the imaging system and image files were created using Spyglass Transform from the output of the MATLAB simulations.

MATLAB (or MATrix LABoratory) is an interactive system and programming language for general scientific and technical computation developed by the Math Works, Inc. [Ref. 11]. The basic data and variable element in MATLAB is a matrix that does not require dimensioning. Programming in MATLAB is simplified by the fact that MATLAB expressions are coded nearly identically to how they are written mathematically.

Spyglass Transform is an image processing package that provides for the creation, manipulation, and display of large image files. Spyglass Transform is a product of Spyglass, Inc., and is available for use on Apple computers and with PC Windows [Ref. 12]. For this simulation, the Apple version was used.

2. Procedure

a. Background

The imaging system was modeled as described by Equation 18. Two programs were written to simulate the operation of the system, IDEAL.M and ACTUAL.M (described later). The code for these programs is provided in the Appendix. The .M extension indicates a MATLAB specific file. These two files are called *script files*. When

39

a *script* file is invoked, MATLAB simply executes the commands found in the file. The statements found in a script file operate globally on the data in the workspace. Additionally, two small *function* files, COSINE.M and CHIRP.M, were written to provide the desired input functions to the input spatial light modulator. *Function* files are subroutines that, unlike *script* files, are able to pass arguments and also operate on variables in a local sense. Variables defined and manipulated inside the file are local to the function and do not operate globally on the workspace [Ref. 11].

b.   Simulation of Ideal SLM

IDEAL.M is written to model a SLM with an ideal linear amplitude-only SLM transmittance with constant phase. This ideal transmittance was used as a reference against which the actual operating characteristics could be compared. The program is set up to take keyboard input of the type of input function desired (cosine or chirp) and the range of gray-scale transmittance, from 0-255, to be modeled for the SLM. The program calculates the transmittance based on this input using an *offset* value that is midway between the input upper and lower gray-scale values and a *gain* value that maintains the maximum values of the function within the specified range. Figure 13 shows the calculated chirp input function that uses the full range (0-255) of gray-scale values. For this gray-scale range, the offset is 127.5 and the gain is also 127.5. Figure 14 shows the linear-amplitude, constant-phase transmittance curves for this ideal amplitude-only SLM. Only one-dimensional functions were considered for this model. Extension to two-dimensions

was accomplished using output from this program and the Spyglass image processing

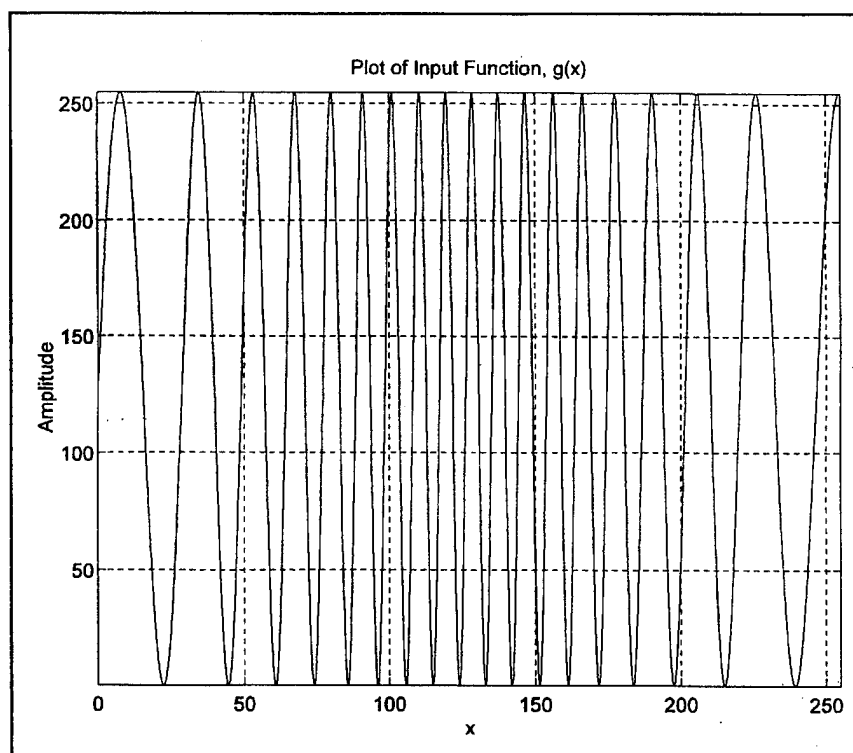package and is discussed in a subsequent section.

Figure 13. Plot of input chirp function for gray-scale 0-255.

At each sample point, the input function values were converted to the closest

realizable integer values by rounding up or down to this value. The complex transmittance

value was found from a look-up table that was implemented as follows. As shown

previously in Tables I and II, 27 discrete data points were measured between 0 and 255

41

gray-scale to determine the complex transmittance of the SLM. The look-up table requires that all the integers between 0 and 255 be represented, so a spline interpolation was performed on the experimentally determined values of the complex operating curve of the liquid crystal cell to obtain interpolated values at each value of the gray-scale. Then, for each rounded value of the input function, the value of the associated interpolated value of the SLM transmittance multiplies that value of the input, which effectively accounts for the complex nature of the SLM transmittance.

For the ideal case considered, the amplitude portion of the transmittance curve was a linear ramp from zero to one in normalized intensity with a constant phase of zero. As previously indicated, these are depicted in Figure 14 for the full range of gray-scale.
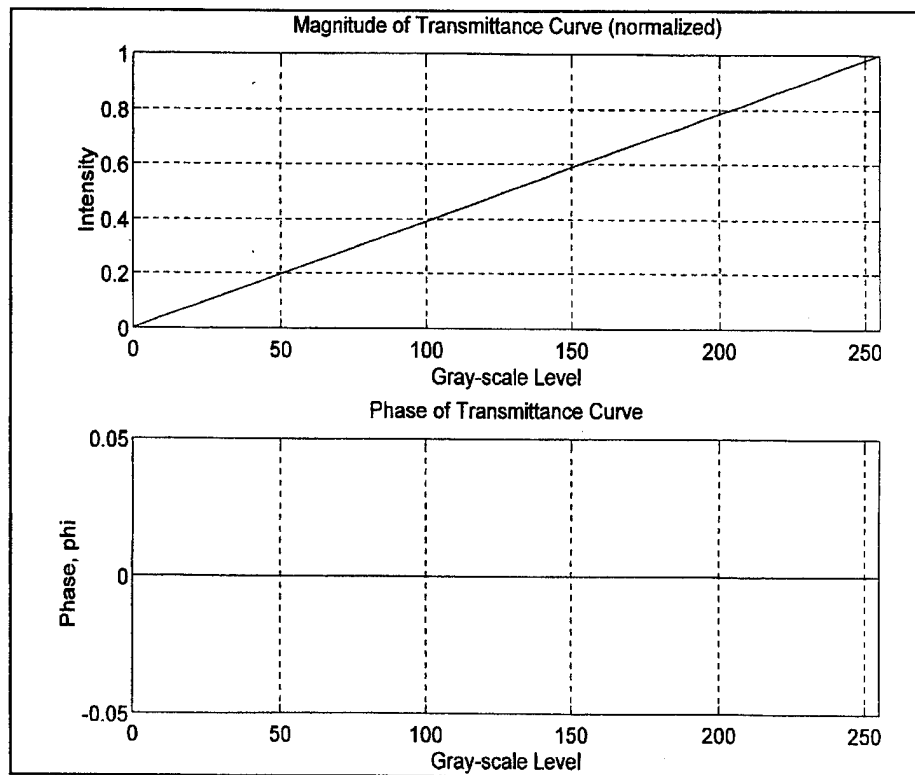

Figure 14. Magnitude and phase plots for ideal SLM operating curve.

Magnitude and phase plots of the output of SLM1 for this transmittance with a linear chirp input (Eq. 17) are shown in Figure 15. Since the output function should equal the input function for the ideal case, we note that the SLM's ideal transmittance provides no distortion to the input function. The phase is uniformly zero as shown in the bottom half of Figure 15.
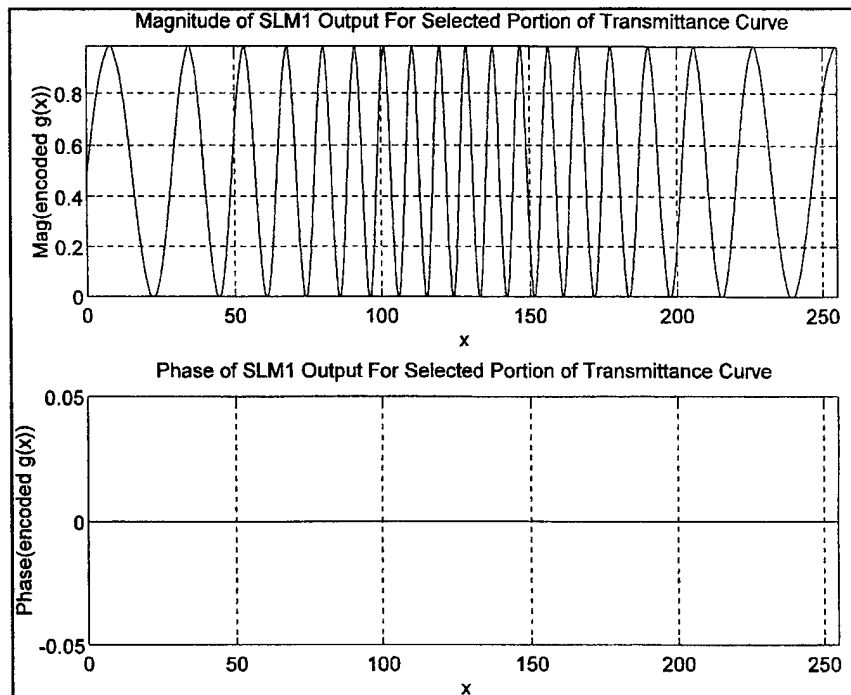

Figure 15. Upper curve is magnitude and lower curve is phase of SLM1 output for ideal operating curve with a linear chirp input.

A Fourier transform of the output of SLM1 was then taken using MATLAB's fast Fourier transform (FFT) function to simulate the Fourier transform performed by the first Fourier transform lens in the system. For vectors with a length that is a power of two, MATLAB uses a fast radix-2 FFT. Since vector lengths in the correlator simulation were all equal to 1024, we were able to take advantage of this feature. The magnitude squared

of the Fourier transformed output of SLM1 is depicted on a linear scale in the top portion

of Figure 16. The lower portion of Figure 16 provides the same plot with the vertical scale

converted to dB to provide better representation of the spectral components of the
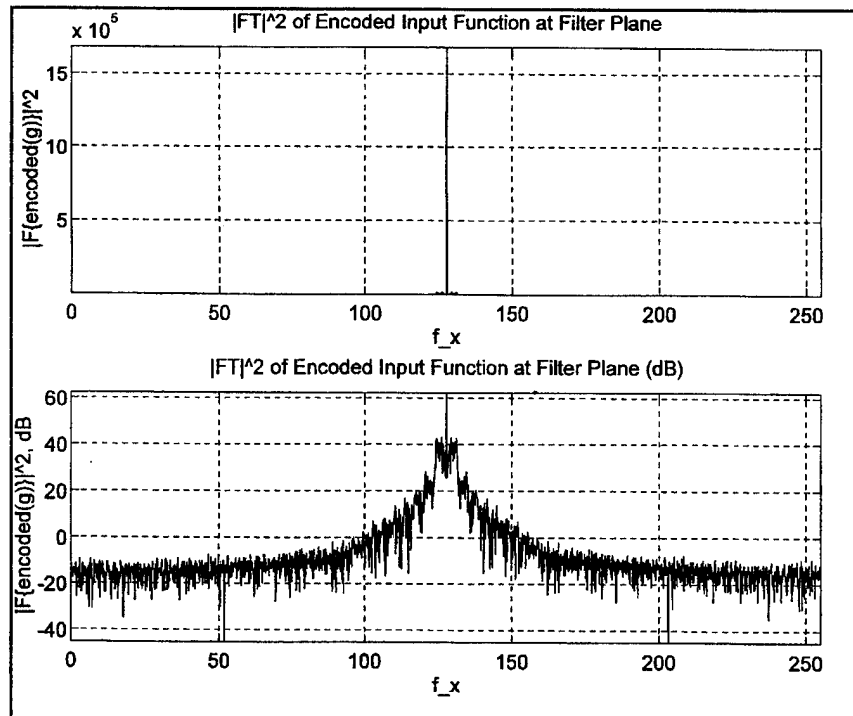
transformed chirp function.

Figure 16. Plot of Fourier magnitude spectrum for chirp function
with amplitude-only transmission of input SLM. Lower portion of
figure is spectrum in dB.

A second FFT is taken by the simulation program to model the operation of the second lens as indicated in Equation 24. The square of the magnitude of this function is then taken, corresponding to intensity detection by the CCD camera in the correlation plane of the actual system. A plot of this intensity function is shown in Figure 17. Since the complex transmittance considered was for that of a linear, amplitude-only SLM, there is, as expected, no distortion of the output intensity function.
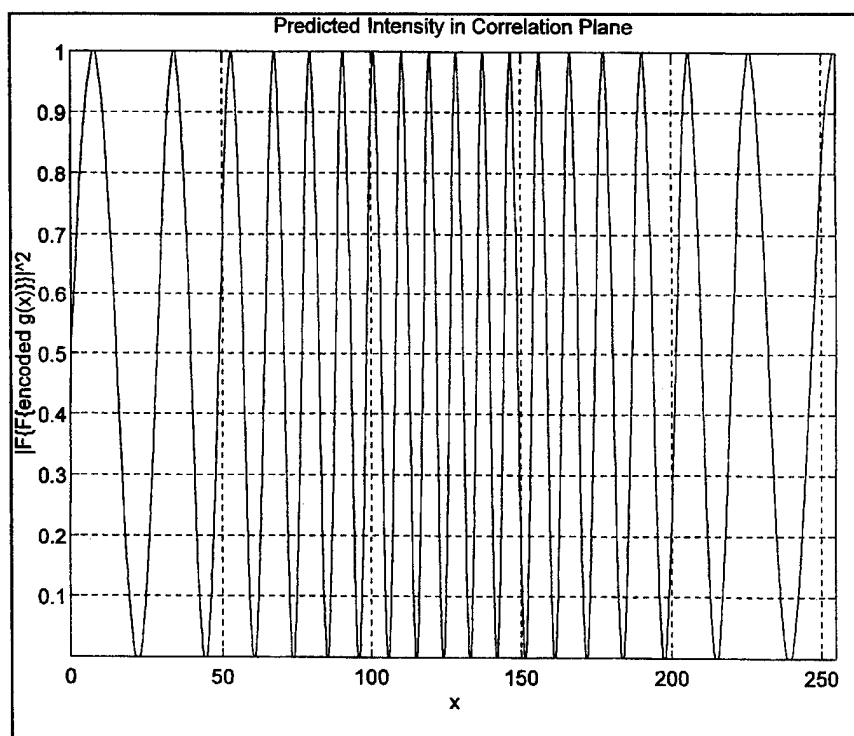

Figure 17. Intensity detected chirp function in correlation plane of imaging system for ideal input SLM.

c. *Simulation of Actual SLM*

ACTUAL.M was written to simulate the measured operating characteristics of the input SLM of the correlator system, using data obtained via the method discussed in Chapter III. Keyboard input to this program is the same as for IDEAL.M. The input function to SLM1 is again calculated based on the range of gray-scale values input by the operator. For input values less than the full range, the value of *offset* is calculated as the midrange of the minimum and the maximum values entered and the value of *gain* is calculated so that the input function ranges between the minimum and maximum values entered. A spline interpolation, using MATLAB's built-in SPLINE function, is again utilized to obtain the input values at each of the gray-scale levels between the minimum and maximum values selected by the operator, so that the effect on the input function by the complex transmittance can be accomplished over the specified range. Figure 18 again shows the chirp function for the full range (0-255) of possible gray-scale values and Figure 19 shows the experimentally obtained amplitude and the phase transmittance measurements for the input SLM.
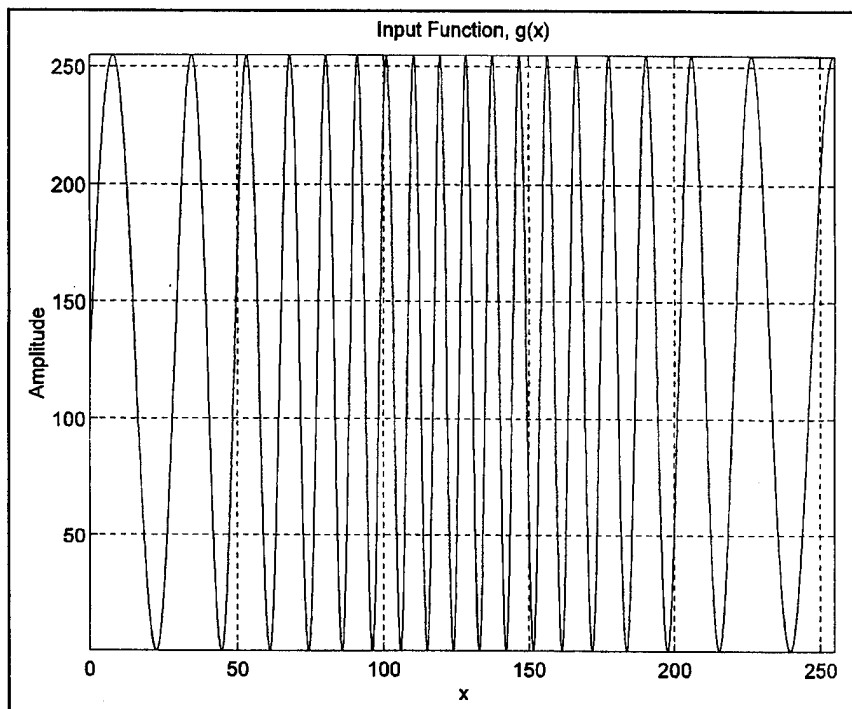
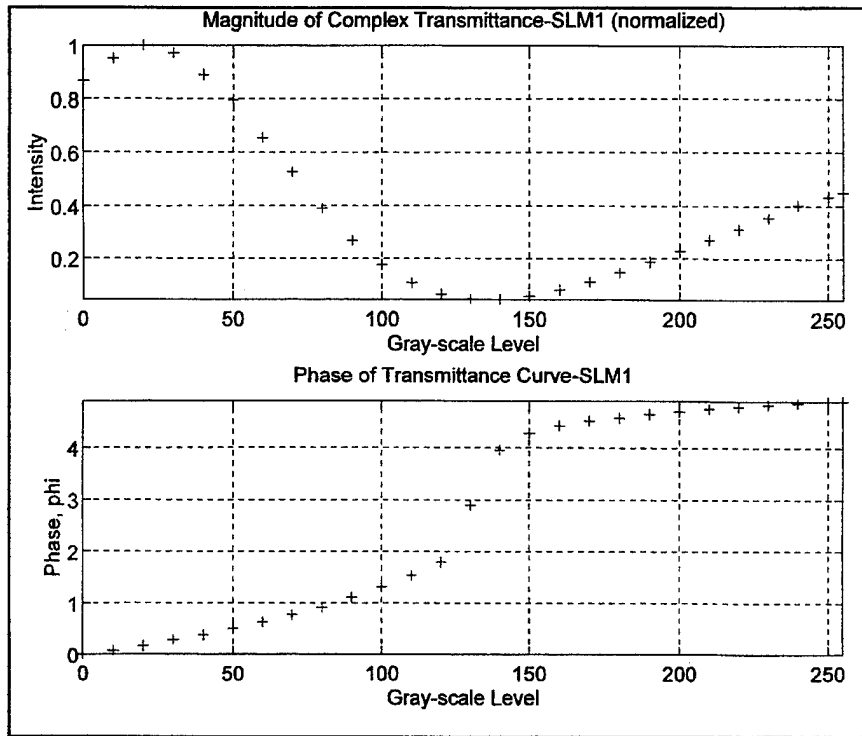Figure 18. Plot of input chirp function.

Figure 19. Magnitude and phase, respectively, of measured transmittance curve for input SLM.

The input function is then converted to the closest realizable integer values by rounding up or down to this value and multiplied by the complex transmittance by use of the spline-interpolation and look-up table, as was done in the ideal case. A plot of the magnitude and phase of the chirp function after this transmittance using the full gray-scale range of 0-255 is shown at Figure 20. There is a contrast reversal and distortion of the input function due to the nonlinear operating characteristics of the SLM.
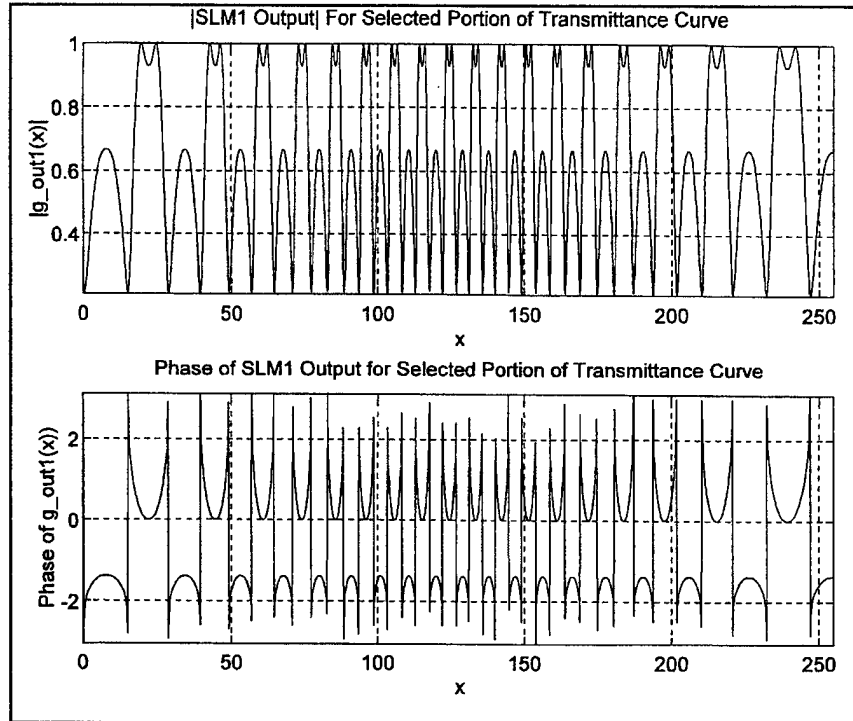
Figure 20. Upper plot is magnitude and lower plot is phase of chirp function at output of SLM1 using the full range of gray-scale.

Figure 21 shows the spatial spectral content in the filter plane, i.e., after the first Fourier transform operation, and Figure 22 shows the distorted signal as it is intensity detected in the correlation plane.

As discussed in Chapter II, we wanted to find a portion of the complex transmittance curve of the input SLM that might have more linear behavior and hence provide less distortion to the input function than that caused by using the full range of

gray-scale. In addition, it was important to maintain good contrast ratio for the function (where "contrast ratio" is defined as the ratio of the maximum transmitted intensity to the minimum transmitted intensity for the full range of gray-scale). The portion of the curve that best met this requirement ranged from a gray-scale of 20 to a gray-scale of 120. Figure 23 illustrates the input chirp function resulting from the selection of gray-scale values ranging from a minimum of 20 to a maximum of 120.
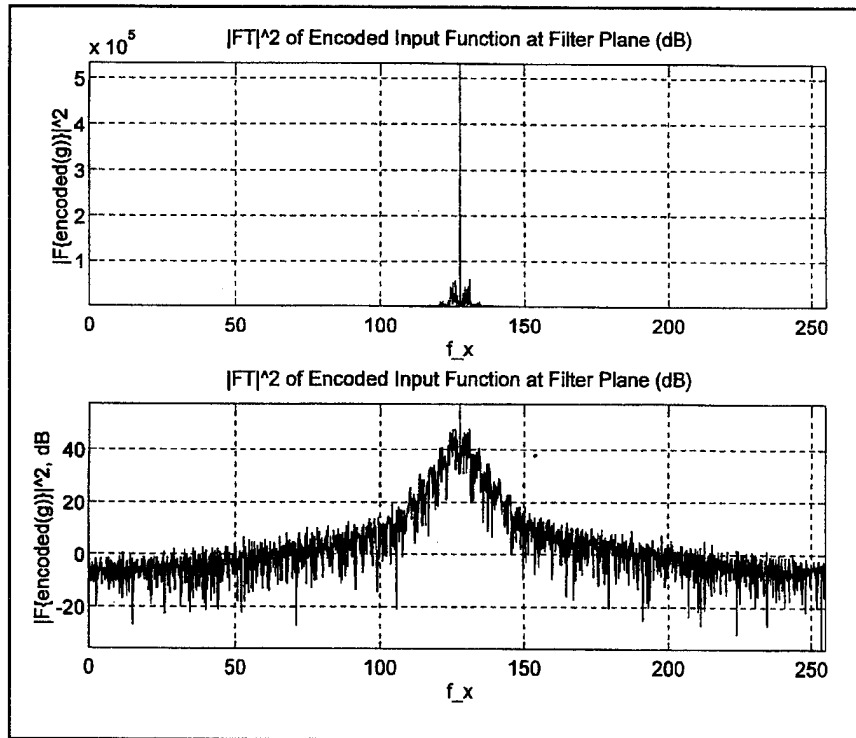

Figure 21. Upper portion is magnitude of spectrum in the imaging system filter plane for a chirp function input for the full-range complex encoding by the input SLM. Lower portion is in dB.
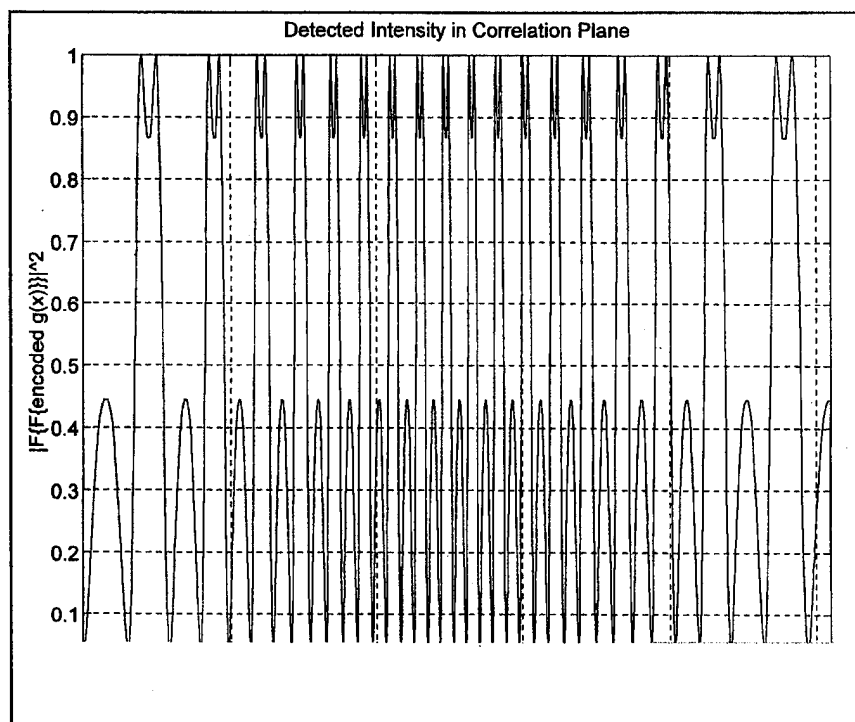
Figure 22. Intensity detected chirp function in correlation plane of imaging system for full complex encoding by input SLM.

Figure 24 depicts the magnitude and phase plots of the portion of the transmittance curve selected by choosing a restricted range of gray-scale values from 20 to 120. The magnitude and phase of the output of SLM1 over the abbreviated range after transmission with the selected portion of the operating curve are shown at Figure 25. Although there is still some distortion of the signal, the distortion is greatly reduced relative to that seen when using the full range of gray-scale values.
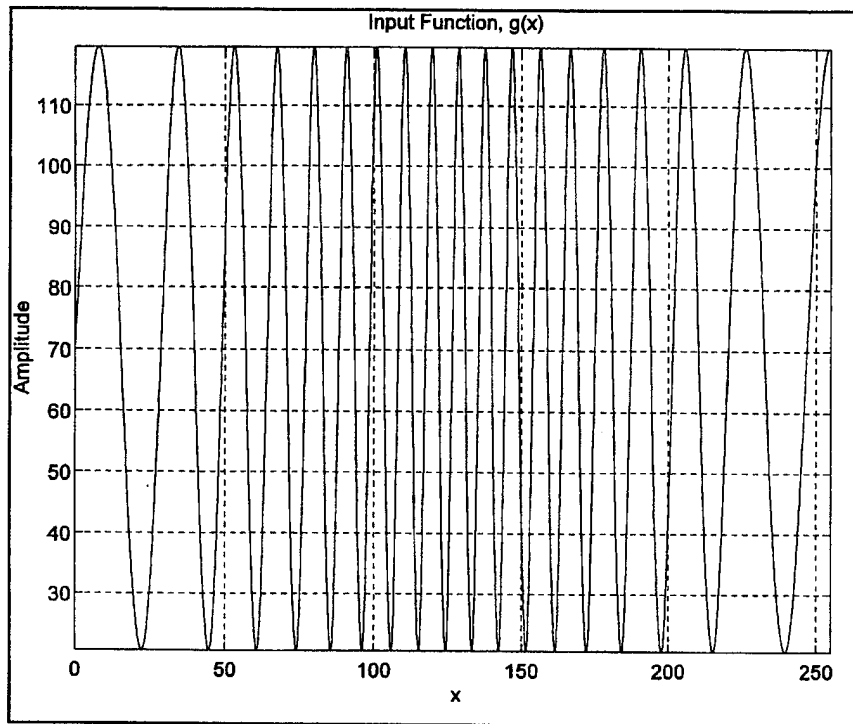
51

Figure 23. Chirp input function for gray-scale values of 20–120.

Figure 26 shows the spectral content in the filter plane and Figure 27 again indicates the reduced amount of distortion of the function that is intensity detected in the correlation plane.
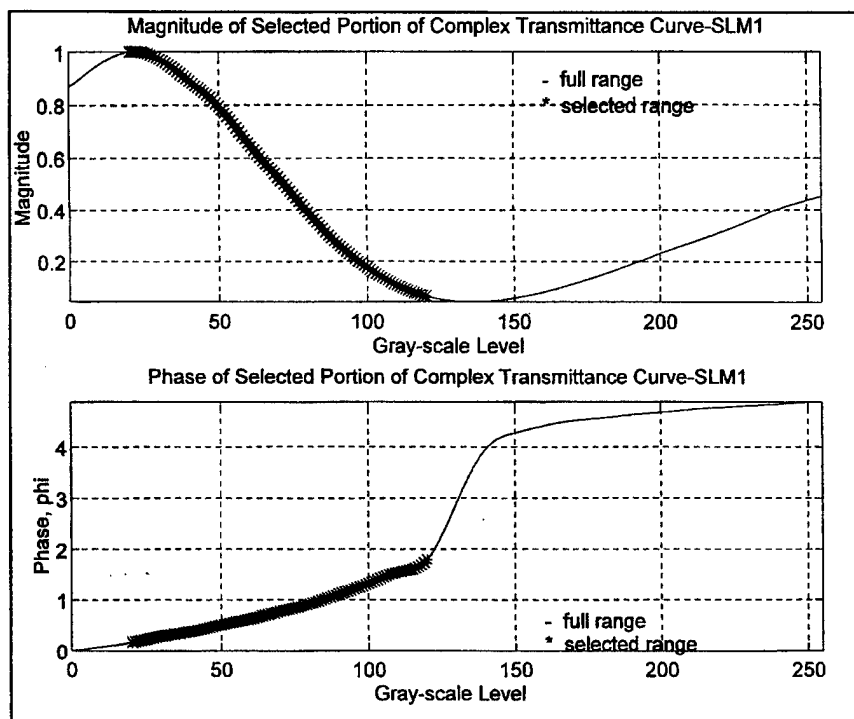
Figure 24. Selected portion of input SLM's complex operating curve for gray-scale values 20-120 (highlighted points). Upper curve is transmittance magnitude and lower curve is transmittance phase.
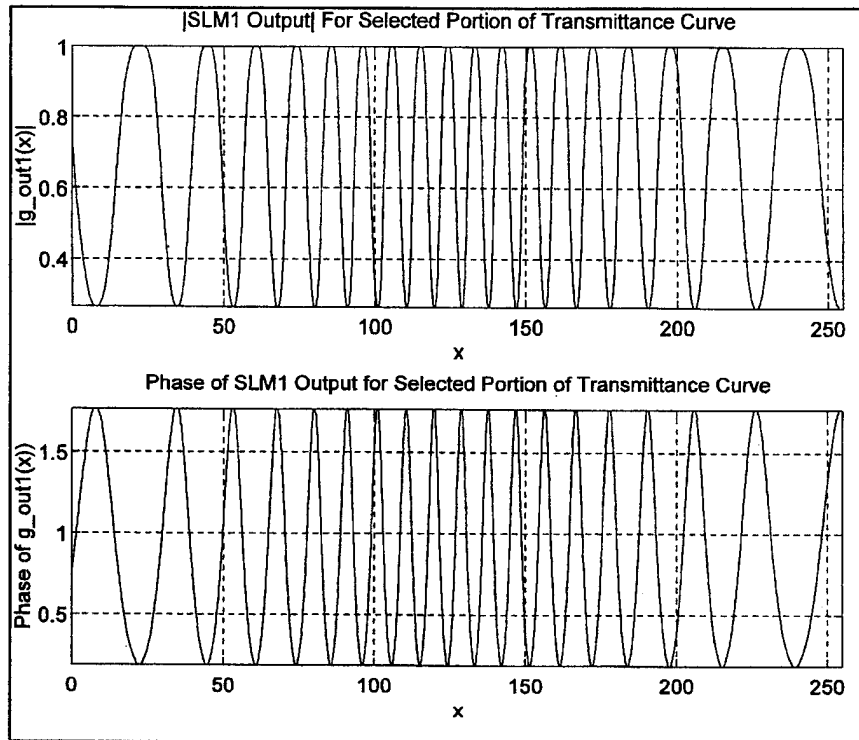
Figure 25. Upper curve is magnitude and lower curve is phase of chirp function at SLM1 output using gray-scale values 20-120.

Figure 26. Fourier spectrum of chirp function in filter plane for complex encoding by input SLM using gray-scale values 10–120. Lower curve is same spectrum in dB.

55

Detected Intensity in Correlation Plane

Figure 27. Detected intensity in correlation plane for chirp function input with complex encoding by SLM1 using piecewise-linear grayscale from 20-120.

d.   Comparison of Ideal and Actual Transmittance Effects
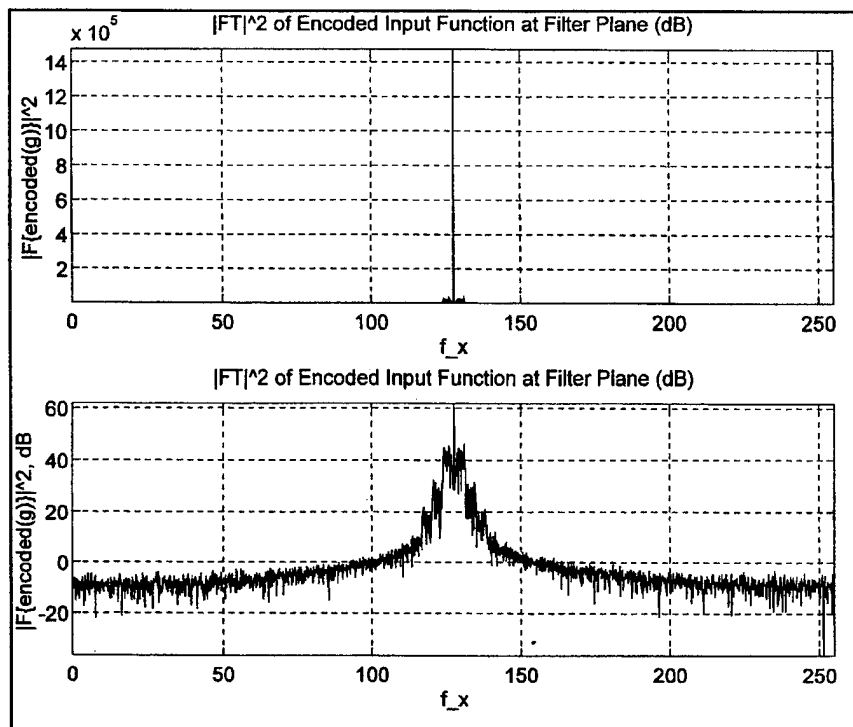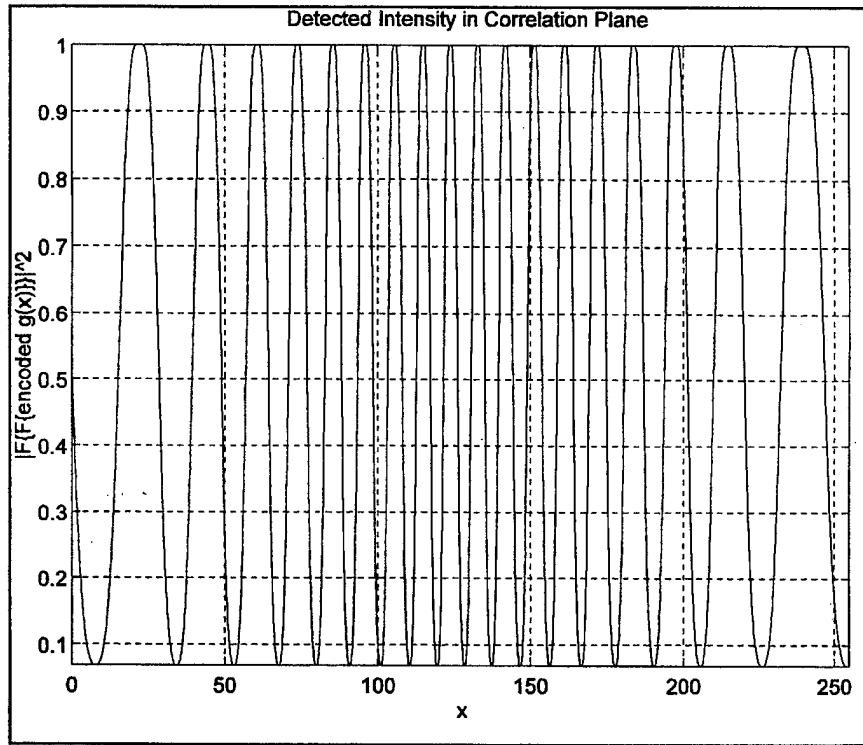
A comparison of the output curves in the correlation plane of the imaging

system for the ideal and actual complex transmittances of the input SLM is provided at

Figure 28 for the full range of possible gray-scale values. In addition to the distortion of

the output for the actual case, there is also a contrast reversal caused by the negative slope

of the actual complex transmittance curve.

Figure 29 illustrates the comparison of the simulated intensity-detected chirp

function in the correlation plane for ideal and actual operating characteristics for the input

SLM for gray-scale values of 20-120. Although there is a marked improvement in

distortion of the signal, there is still a contrast reversal due to the fact that the selected

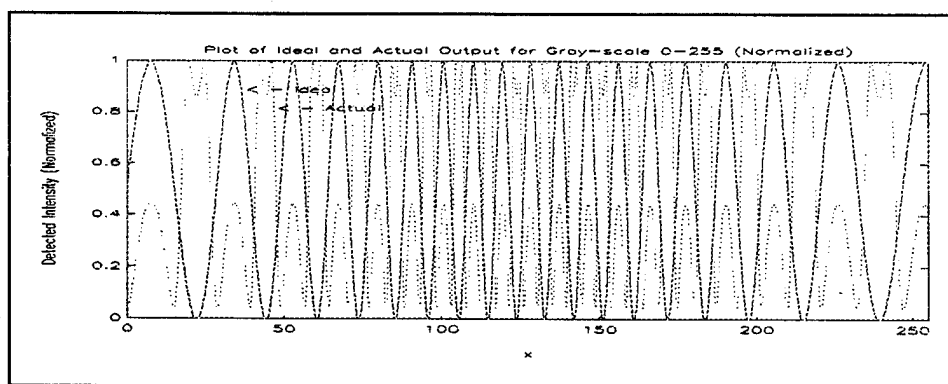portion of the operating curve has negative slope.

Figure 28.   Comparison of simulated correlator output for the ideal
transmittance and the actual SLM transmittance gray-scale values 0-255.
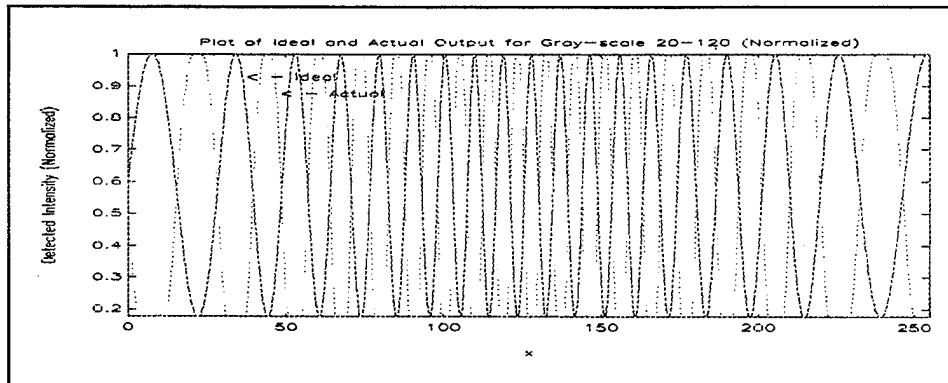
Figure 29. Comparison of simulated correlator system outputs for ideal transmittance and measured SLM transmittance using piecewise-linear portion from 20–120.

E.   EXTENSION TO IMAGE FILES

1.   One-dimensional Chirp

The generation of image files for a one-dimensional chirp was accomplished using a combination of MATLAB and Spyglass Transform functions to serve as a baseline for verification of imaging system simulation performance. A windowed average (i.e., the average value over 4 samples) was taken for all the values of the chirp function from 1 to 1024 to obtain a 256-element sampled vector. A 256x256 one-dimensional chirp array was created by writing the 256-element sampled vector to 256 separate rows using the CHIRP.M file listed in the Appendix. The MATLAB SAVE command saved this array in ASCII format. This saved file was then read into Spyglass Transform where an image of the array was created.

Because of the double slope reversal of the amplitude of the input SLM's complex

transmittance curve, the one-dimensional chirp was evaluated using the piecewise linear

region of the SLM transmittance corresponding to 20-120 gray-scale range. Figure 30 is

the 256x256 simulated one-dimensional chirp input to SLM1 using the 20-120 gray-scale

range. Figure 31 shows the output of the imaging simulation over the same range. As

expected from the previous simulation results, there is a reversal of contrast that manifests

itself as an inversion of gray-scale between the input and output images.
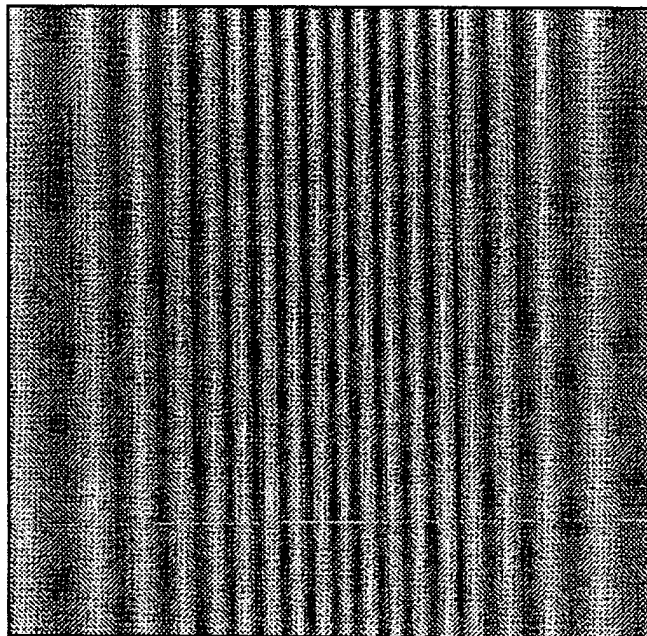
Figure 30. One-dimensional chirp image input to
SLM1 for gray-scale 20-120.
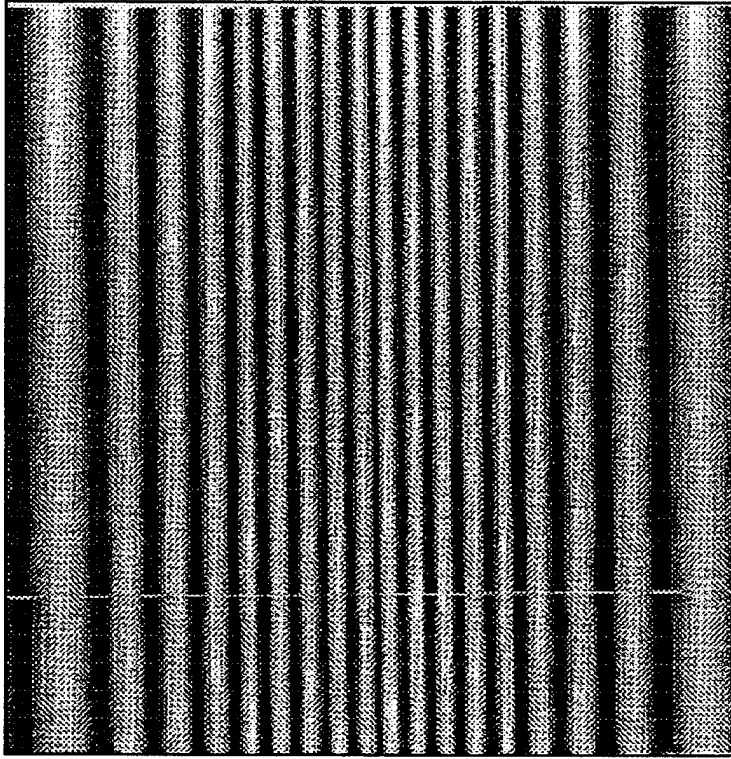
Figure 31. Output one-dimensional chirp image for gray-scale 20-120.

2. Two-dimensional Chirp

Development of image files for a two-dimensional chirp function was accomplished using MATLAB's built-in MESHDOM function. The function MESHDOM transforms the domains specified by vectors x and y into arrays XX and YY for evaluating functions of two variables. To emulate the resolution of the SLMs, the chirp function of length 1024 was again converted to a 256 element vector by averaging over successive groups of 4 samples, each from 1 to 1024, providing a windowed average for the 256 element vector.

In this case, two identical 256 element chirp vectors were transformed by MESHDOM into two 256x256 arrays. These were then multiplied element-by-element to create a 256x256 two-dimensional chirp array. This array was then saved as an ASCII file in the same manner as for the one-dimensional case, loaded by Spyglass Transform, and converted to a 256x256 image.

Figure 32 shows the simulated two-dimensional chirp image input to the imaging simulation for a gray-scale of 0 to 255. Figure 33 is the simulated two-dimensional output image from the simulation using the entire gray-scale range of the SLM transmittance. Figure 33 shows the effects of the distortion caused by the complex operating characteristics of SLM1.
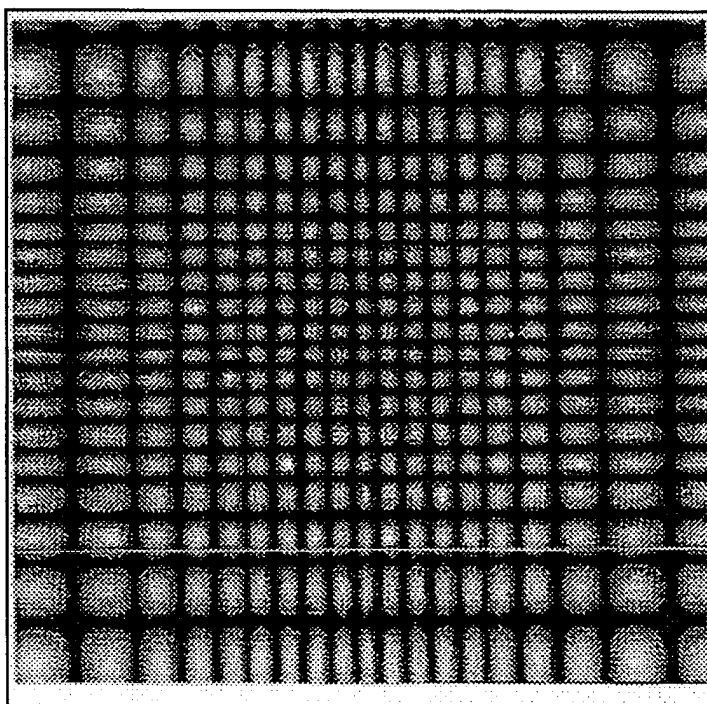
Figure 32. Simulated two-dimensional input chirp function for gray-scale 0-255.
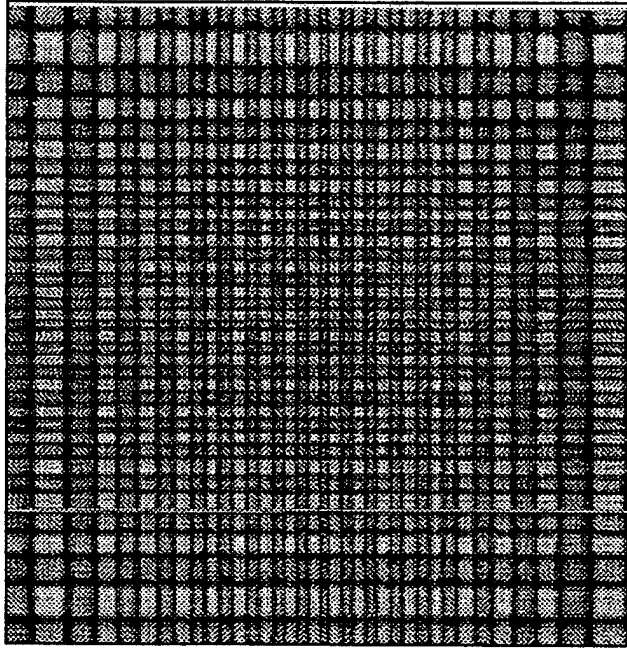
Figure 33. Simulated two-dimensional chirp
output image for gray-scale 0-255.

Figures 34 is the input image from the actual imaging sytem for a gray-scale range

of 0-255 and Figure 35 is the corresponding output image for the same gray-scale range.

The predicted contrast reversal and amplitude distortion of the output image are clearly

evident.
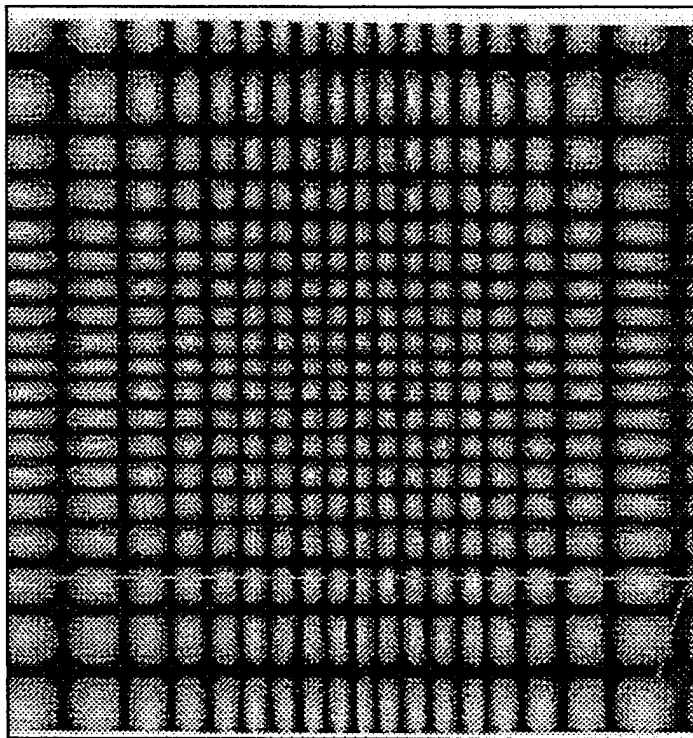
Figure 34. Actual imaging system input chirp image for gray-scale 0-255.
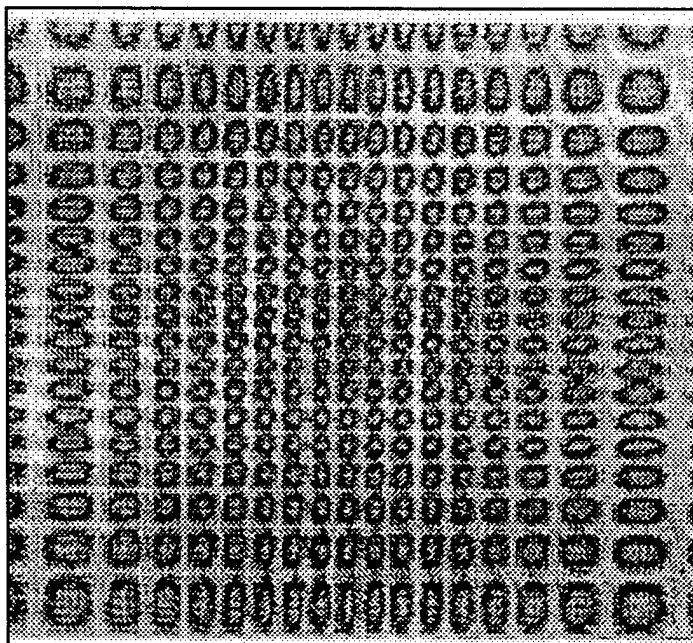
Figure 35. Actual imaging system two-dimensional chirp output with gray-scale 0-255.

63

Figure 36 is the two-dimensional simulated chirp input to the imaging simulation for gray-scale values 20-120. Figure 37 is the predicted intensity output in the correlation plane for the same simulated chirp function. Inspection of the two images indicates the expected contrast reversal. The bright areas are those corresponding to maximum gray-scale, 120 in this case, and it is clear that as seen in the one-dimensional case, these shift by one half cycle from the input to the output.
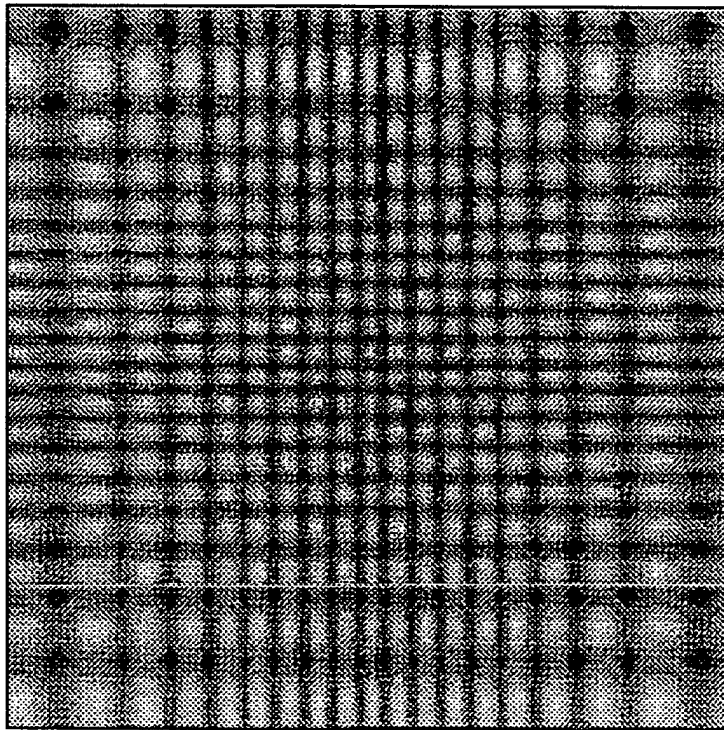
Figure 36. Input two-dimensional chirp input to imaging simulation for gray-scale 20-120.

Figures 38 and 39 provide image data actually taken from the imaging system in the same configuration as that assumed by the simulation. Figure 38 is the input two-dimensional chirp image to SLM1 for gray-scale values 20-120. Figure 39 is the intensity

detected output image over the same range. Comparison of these images indicates the expected contrast reversal manifests itself in a different manner than the simulated results but is evident nevertheless. More importantly, it shows that the distorting effects caused by the complex transmittance of the liquid crystal cell can be mitigated by careful selection of an appropriate region of the operating curve.

The results obtained from the simulation of the correlator as an imaging system indicate that the LCTV SLMs can be modelled and their behavior reasonably predicted with the simulation software. Chapter V summarizes the results of the thesis and discusses areas of potential future work using these spatial light modulators in correlator applications.

Figure 37. Intensity detected output image for imaging simulation for gray-scale 20-120.
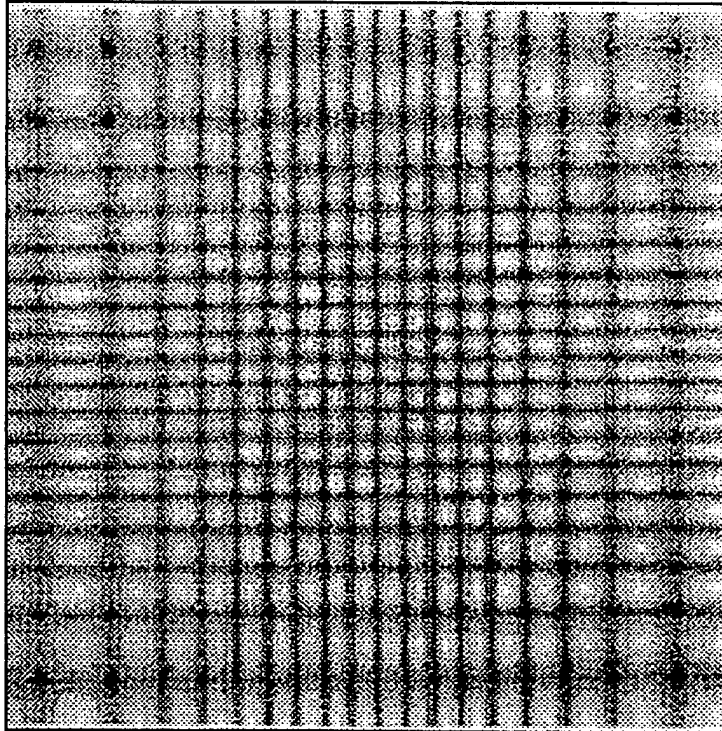
Figure 38. Input image for actual imaging system for gray-scale 20-120.
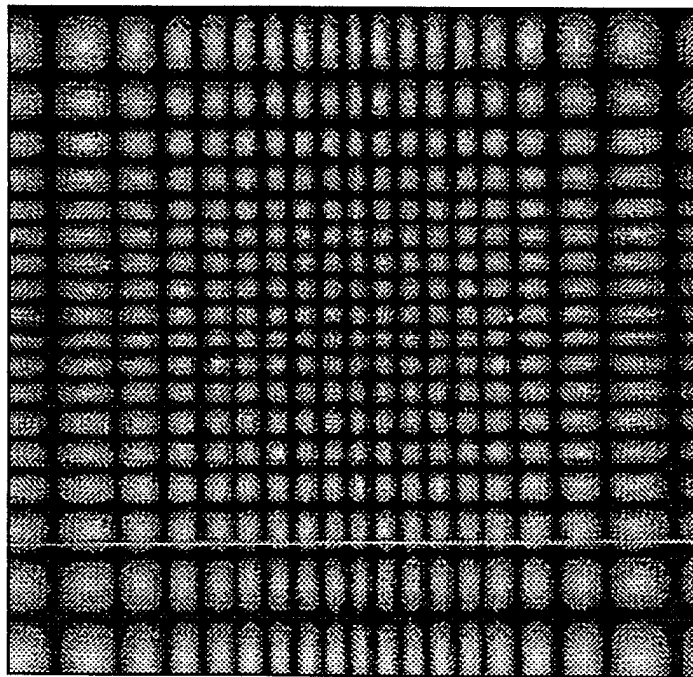
Figure 39. Intensity detected output image for actual imaging system for gray-scale 20-120.

66

V. SUMMARY

This thesis demonstrated the effects of the complex transmittance of liquid crystal television spatial light modulators on an optical correlator configured as an imaging system. A model was developed to simulate this system using LCTV SLMs and was used to evaluate their eff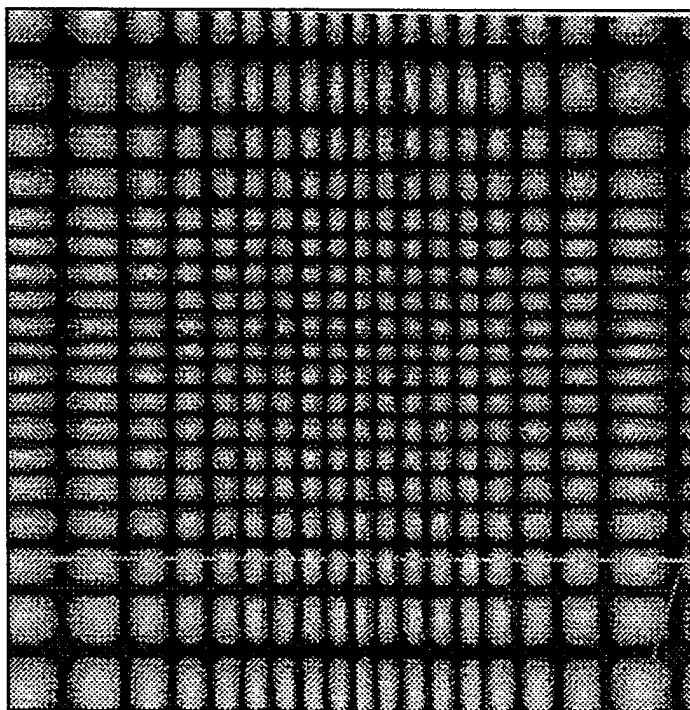ect on known input functions. Measured image data confirmed the performance of the model. The simulation provided a reliable method for predicting the effects of complex transmittance on image quality in an optical correlator configured in this manner.

The simulation was also set-up to provide the operator a capability to observe effects caused by selective utilization of the complex transmittance curve. Analysis showed that it is possible to control the adverse effects of the SLMs nonlinear transmittance on a function that is processed by the imaging system by choosing a piecewise linear region of the transmittance curve and controlling the dynamic range of the input signal to match the piecewise region. Of note is the fact that, although the effects of the phase characteristics of the SLMs transmittance have no impact on the correlator output when configured as an imaging system, these effects would be significant in an actual correlator.

Optical correlation shows great promise for future applications requiring the increased speed and efficiency afforded by optical processing. The advent of cheaper, more readily available means of providing filters and input image data to correlators will make their use increasingly competitive with pure digitally processed imaging systems.

Future thesis study could focus on adding the effects of a second SLM, e.g., at the correlator filter plane, on the processing of an image and relating noise variance in the correlation plane to complex transmittance of the filter plane.

APPENDIX. MATLAB CODE FOR IMAGING SIMULATION

The following programs were used to simulate the operation of the Hybrid Vision

Lab optical correlator configured for the imaging application. IDEAL.M implemented the

amplitude-only, ideal characteristics for the operating curve of SLM1. This was used for

comparison with data from the actual SLM characterization. ACTUAL.M was the code

that implemented the experimentally obtained data from the characterization of the liquid

crystal cell using Soutar's method. COSINE.M and CHIRP.M were MATLAB function

programs called by the other two to provide the input functions to the imaging system.

IDEAL.M SOURCE CODE

```
%%%%
%%%%
%%%%    Program ideal.m                                    March 1993
%%%%
%%%%
%%%%    This program simulates the operation of an optical imaging system
%%%%    illuminated by a plane wave. It computes the complex transmittance
%%%%    of the input SLM1 from the chosen cosine or chirp input function
%%%%    and the desired gray-scale range selected by the operator. From
%%%%    these inputs it calculates and plots
%%%%
%%%%        1) the input function
%%%%        2) the complex transmittance over the specified range
%%%%        3) the wave at the filter plane
%%%%        4) the spatial transform of the wave at the filter plane, and
%%%%        5) the predicted intensity at the correlation plane (assuming
%%%%                    an ideal filter SLM2).
%%%%
%%%%    This program simulates the imaging system performance if spatial
%%%%    light modulators with ideal transmittance were used.
%%%%
%%%%

! del homey*.met
clg


I=linspace(0,1,27);
phi=zeros(I);
```

```
func=input('Select input function-(0 for cosine, 1 for chirp) [1]:  ');
if isempty(func), func=1; end


disp(' '),disp(' '),disp(' '),
disp(' Select desired lower limit of transmittance curve ');
disp(' in gray-scale level')
l1=input('(0-240 in increments of 10) [0]:  ');

if isempty(l1),  l1=0;
elseif l1 < 0,   disp(' Error.  Limit out of range. ')
elseif l1 > 240, disp(' Error.  Limit out of range. ')
end

disp(' '),disp(' '),disp(' '),
disp(' Select desired upper limit of transmittance curve ');
disp(' in gray-scale level')
l2=input('(10-250 in increments of 10 or the value 255) [255]:  ');

if isempty(l2),  l2=255;
elseif l2 < 10,  disp(' Error.  Limit out of range. ')
elseif l1 > 255, disp(' Error.  Limit out of range. ')
end

if l1 > l2, disp(' Error.  Lower limit must be less than upper limit ')
elseif l1 = l2, disp(' Error.  This is a meaningless example in this ');
disp('simulation. ')
end

%%%%  Calculates gain and offset from input values

N=256;                     %%%%  Number of sample points
offset=(l1+l2)/2;          %%%%  Offset to center function between
                           %%%%  upper and lower gray-scale bounds
gain=(offset-l1)-0.5;      %%%%  Gain controls maximum and minimum values
                           %%%%  that may be attained by function

%%%%  Calls function subprograms "chirp.m" or "cosine.m"; returns the
%%%%  appropriate function as a vector and the length of that vector

if func == 0,
     [g,x]=cosine(offset,gain,N);
else [g,x]=chirp(offset,gain,N);
end


%%%%  Defines the complex transmittance curve of the Spatial Light
%%%%  Modulator for the upper and lower gray-scale bounds given

n=length(g);
j=sqrt(-1);
if l2 == 255
   v=[l1:10:250 255];
   c=sqrt(I(ceil(l1/10+1:l2/10+2))).*exp(j*phi(round(l1/10+1:l2/10+2)));
else
   v=[l1:10:l2];
```

70

```
c=sqrt(I(ceil(l1/10+1:l2/10+1))).*exp(j*phi(round(l1/10+1:l2/10+1)));
end

vi=[l1:l2];
ci=spline(v,c,vi);

if l1 == 0,         %%%%  Changes range of gray-scale from 0 -> 255
     l1=l1+1;       %%%%  to 1 -> 256 for indexing
     l2=l2+1;
end


%%%%  Multiplies unit-amplitude plane wave (1+j0) by the complex
%%%%  transmittance of the Spatial Light Modulator

for i=1:n,
     e(i)=ci(round(g(i)-(l1-1)));
end

%%%%  Plot of input function

gsl=linspace(0,255,27);
ax_1=[min(x),max(x),min(g),max(g)];
axis(ax_1),plot(x,g),grid,
title(' Plot of Input Function, g(x) '),
xlabel(' x '),ylabel(' Amplitude '),pause
meta homey1a

ax_2=[min(gsl),max(gsl),min(I),max(I)];
ax_3=[min(gsl),max(gsl),-.05,.05];
axis(ax_2),subplot(211),plot(gsl,I),
title('Magnitude of Transmittance Curve (normalized)'),
xlabel('Gray-scale Level'),ylabel('Intensity')
axis(ax_3),subplot(212),plot(gsl,phi),
title('Phase of Transmittance Curve')
xlabel('Gray-scale Level'),ylabel('Phase, phi'),pause
meta homey1b

%%%%  Plot of SLM1 output with encoding from selected portion of complex
%%%%  transmittance (i.e. desired linear region) displayed versus full
%%%%  range of complex transmittance

if l1==1, l1=l1-1; l2=l2-1; %%%%  Sets range back to 0 -> 255   (if
end                         %%%%  required)

full_gsl=0:255;
full_I=spline(gsl,I,full_gsl);
full_phi=spline(gsl,phi,full_gsl);

clg
ax_10=[min(full_gsl),max(full_gsl),min(full_I),max(full_I)];
ax_11=[min(full_gsl),max(full_gsl),-.05,.05];

axis(ax_10),
subplot(211),
plot(full_gsl,full_I,full_gsl(l1+1:l2+1),full_I(l1+1:l2+1),'*'),
```

```
title('Magnitude of Selected Portion of Transmittance Curve-SLM1'),
ylabel('Intensity'),xlabel('Gray-scale Level'),
text(160,.9,'-  full range'),text(160,.8,'*  selected range')

axis(ax_11),
subplot(212),
plot(full_gsl,full_phi,full_gsl(l1+1:l2+1),full_phi(l1+1:l2+1),'*'),
title('Phase of Selected Portion of Transmittance Curve-SLM1'),
ylabel('Phase, phi'),xlabel('Gray-scale Level'),
text(160,-.03,'-  full range'),text(160,-.04,'*  selected range'),pause
meta homey2


%%%%  Displays effect of output of SLM1 on the input function

clg
ax_4=[min(x),max(x),min((abs(e)).^2),max((abs(e)).^2)];
axis(ax_4),subplot(211),plot(x,(abs(e)).^2),grid, .
title('Magnitude of SLM1 Output For Selected Portion of Transmittance
     Curve'),
ylabel('Mag(encoded g(x))'),xlabel('x')

ax_5=[min(x),max(x),-.05,.05];
axis(ax_5),
subplot(212),plot(x,angle(e)),grid,
title('Phase of SLM1 Output For Selected Portion of Transmittance
     Curve'),
ylabel(' Phase(encoded g(x)) '),xlabel('x'),pause
meta homey3



%%%%  Calculates and plots the Fourier transform of the SLM1 output as
%%%%  seen at the filter plane of the imaging system

clg
E=fft(e);
ax_6=[min(x),max(x),min(abs(E).^2),max(abs(E).^2)];axis(ax_6),
subplot(211),plot(x(1:length(E)),fftshift((abs(E)).^2)),
title(' MAG^2 of FT of Encoded Input Function at Filter Plane'),
xlabel(' fx  '),ylabel('|F{encoded(g)}|^2 ')

ax_7=[min(x),max(x),min(10*log10(abs(E).^2)),max(10*log10(abs(E).^2))];a
xis(ax_7),
subplot(212),plot(x(1:length(E)),fftshift(10*log10((abs(E)).^2))),grid,
title(' MAG^2 FT of Encoded Input Function at Filter Plane(dB)'),
xlabel(' f_x  '),ylabel(' |F{encoded(g)}|^2, dB '),pause
meta homey4

%%%%  Calculates and plots the second Fourier transform of the encoded
%%%%  signal as seen at the correlation plane of the imaging system

clg
new_e=fliplr(fft(E));

mod_new_e=new_e(1:length(x));
yy=linspace(0,255,length(mod_new_e));
abs_mod_new_e=(abs(mod_new_e)).^2;
norm_abs_mod_new_e=abs_mod_new_e/max(abs_mod_new_e);
```

72

```
ax_8=[0,max(yy),min(norm_abs_mod_new_e),max(norm_abs_mod_new_e)];
axis(ax_8),plot(yy,norm_abs_mod_new_e),grid
title(' Predicted Intensity in Correlation Plane'),
xlabel(' x '),ylabel(' |F{F{encoded g(x)}}|^2 ')

meta homey5
axis;
```

ACTUAL.M SOURCE CODE

```
%%%%
%%%%
%%%%   Program actual.m                                        March 1993
%%%%
%%%%
%%%%   This program simulates the operation of an optical imaging system
%%%%   illuminated by a plane wave. It computes the complex transmittance
%%%%   of the input SLM1 from the chosen cosine or chirp input function
%%%%   and the desired gray-scale range selected by the operator.  From
%%%%   these inputs it calculates and plots
%%%%
%%%%      1) the input function
%%%%      2) the complex transmittance over the specified range
%%%%      3) the wave at the filter plane
%%%%      4) the spatial transform of the wave at the filter plane, and
%%%%      5) the predicted intensity at the correlation plane (assuming
%%%%                  an ideal filter SLM2).
%%%%
%%%%   This program simulates the actual imaging system performance using
%%%%   the non-linear transmittance of the spatial light modulators.
%%%%
%%%%

!del homey*.met
clg

%%%%   Input measured complex transmittance of SLM1

I=[.8676 .9529 1 .9735 .8912 .7941 .6559 .5265 .3912 .2691 ...
.1765 .1082 .0665 .0471 .0459 .0588 .0818 .1124 .1485 .1888 ...
.2294  .2712 .3118 .3559 .4029 .4353 .4529];

phi=[0 .0729 .1655 .2849 .3777 .5034 .6228 .7684 .9143 ...
1.1063 1.3116 1.5369 1.7881 2.894 3.9547 4.2721 4.4187 ...
4.5181 4.5704 4.6367 4.6838 4.7431 4.7833 4.8234 4.8565 ...
4.8897 4.8949];

func=input('Select input function-(0 for cosine, 1 for chirp) [1]:  ');
if isempty(func), func=1; end

disp(' '),disp(' '),disp(' '),
disp(' Select desired lower limit of transmittance curve in gray-scale
     level')
ll=input('(0-240 in increments of 10) [0]:  ');
```

```
if isempty(l1)
      l1=0;
elseif l1 < 0
      disp(' Error.   Limit out of range. ')
elseif l1 > 240
      disp(' Error.   Limit out of range. ')
end

disp(' '),disp(' '),disp(' ')
disp(' Select desired upper limit of transmittance curve in gray-scale
      level')
l2=input('(10-250 in increments of 10 or the value 255) [255]:   ');
if isempty(l2)
      l2=255;
elseif l2 < 10
      disp(' Error.   Limit out of range. ')
elseif l1 > 255
      disp(' Error.   Limit out of range. ')
end

if l1 > l2,
      disp(' Error.   Lower limit must be less than upper limit ')
elseif l1 = l2, disp(' Error.   This is a meaningless example in this ');
disp('simulation. ')
end


%%%%   Calculates gain and offset from input values

N=256;                      %%%%   Number of sample points
offset=(l1+l2)/2;           %%%%   Offset to center function between
                            %%%%   upper and lower gray-scale bounds
gain=(offset-l1)-0.5;       %%%%   Gain controls maximum and minimum values
                            %%%%   that may be attained by function

%%%%   Calls function subprograms "chirp.m" or "cosine.m"; returns the
%%%%   appropriate function as a vector and the length of that vector

if func == 0, [g,x]=cosine(offset,gain,N);
else [g,x]=chirp(offset,gain,N);
end

%%%%   Defines the complex transmittance curve of the SLM for given upper
%%%%   and lower gray-scale bounds

n=length(g);
j=sqrt(-1);
if l2 == 255
 v=[l1:10:250 255];
 c=sqrt(I(ceil(l1/10+1:l2/10+2))).*exp(j*phi(round(l1/10+1:l2/10+2)));
else
 v=[l1:10:l2];
 c=sqrt(I(ceil(l1/10+1:l2/10+1))).*exp(j*phi(round(l1/10+1:l2/10+1)));
end

vi=[l1:l2];
ci=spline(v,c,vi);
```

74

```
if l1 == 0,            %%%%   Changes range of gray-scale from
l1=l1+1;               %%%%   0 -> 255 to 1 -> 256 for
  l2=l2+1;             %%%%   indexing
end


%%%%  "Encodes" function with the complex transmittance curve of the SLM
for i=1:n, e(i)=ci(round(g(i)-(l1-1))); end

%%%%   Plot of input vector and complex transmittance curve of input SLM
gsl=[0:10:250 255];
ax_1=[min(x),max(x),min(g),max(g)];
axis(ax_1),plot(x,g),grid,title(' Input Function, g(x) '),
xlabel(' x '),ylabel(' Amplitude '),pause
meta homey1a

ax_2=[min(gsl),max(gsl),min(I),max(I)];
ax_3=[min(gsl),max(gsl),min(phi),max(phi)];
axis(ax_2),subplot(211),plot(gsl,I,'+'),
title('Magnitude of Complex Transmittance-SLM1 (normalized)'),
xlabel('Gray-scale Level'),ylabel('Intensity')
axis(ax_3),subplot(212),
plot(gsl,phi,'+'),title('Phase of Transmittance Curve-SLM1')
xlabel('Gray-scale Level'),ylabel('Phase, phi'),pause
meta homey1b


%%%%   Plot input function with encoding from selected portion of complex
%%%%   transmittance curve (i.e. desired linear region) displayed versus
%%%%   full range of complex transmittance

if l1==1,l1=l1-1;l2=l2-1;   %%%%   Sets range back to 0 -> 255   (if
else,l1=l1;l2=l2;end        %%%%   required)

%%%%   Fill in gaps between measured data with spline interpolation

full_gsl=0:255;
full_I=spline(gsl,I,full_gsl);
full_phi=spline(gsl,phi,full_gsl);

clg
ax_4=[min(full_gsl),max(full_gsl),min(full_I),max(full_I)];
ax_5=[min(full_gsl),max(full_gsl),min(full_phi),max(full_phi)];

axis(ax_4),subplot(211),
plot(full_gsl,full_I,full_gsl(l1+1:l2+1),full_I(l1+1:l2+1),'*'),
title('Magnitude of Selected Portion of Complex Transmittance
     Curve-SLM1'),
ylabel('Magnitude'),xlabel('Gray-scale Level'),
text(160,.9,'-  full range'),text(160,.8,'*  selected range')

axis(ax_5),subplot(212),
plot(full_gsl,full_phi,full_gsl(l1+1:l2+1),full_phi(l1+1:l2+1),'*'),
title('Phase of Selected Portion of Complex Transmittance Curve-SLM1'),
ylabel('Phase, phi'),xlabel('Gray-scale Level'),
text(160,.6,'-  full range'),text(160,.15,'*  selected range'),pause
meta homey2
```

```
%%%%   Displays effect of complex transmittance on the input function

clg
ax_6=[min(x),max(x),min(abs(e)),max(abs(e))];axis(ax_6),
subplot(211),plot(x,abs(e)),grid,
title('Magnitude of SLM1 Output For Selected Portion of Transmittance
     Curve'),
ylabel('Mag(encoded g(x))'),xlabel('x')

ax_7=[min(x),max(x),min(angle(e)),max(angle(e))];axis(ax_7),
subplot(212),plot(x,angle(e)),grid,
title('Phase of SLM1 Output For Selected Portion of Transmittance
     Curve'),
ylabel(' Phase(encoded g(x)) '),xlabel('x'),pause
meta homey3


%%%%   Calculates and plots the Fourier transform of the encoded signal
%%%%   as seen at the filter plane of the imaging system

clg
E=fft(e);
ax_8=[min(x),max(x),min(abs(E).^2),max(abs(E).^2)];axis(ax_8),
subplot(211),plot(x(1:length(E)),fftshift((abs(E)).^2)),grid,
title(' MAG^2 of FT of Encoded Input Function at Filter Plane (dB)'),
xlabel(' f_x  '),ylabel('|F{encoded(g)}|^2 ')

ax_9=[min(x),max(x),min(10*log10(abs(E).^2)), ...
     max(10*log10(abs(E).^2))];
axis(ax_9),
subplot(212),plot(x(1:length(E)),fftshift(10*log10((abs(E)).^2))),grid,
title(' MAG^2 FT of Encoded Input Function at Filter Plane(dB)'),
     xlabel(' f_x  '),
ylabel(' |F{encoded(g)}|^2, dB '),pause
meta homey4

%%%%   Calculates and plots the second Fourier transform of the encoded
%%%%   signal as seen at the correlation plane of the system

clg
new_e=fliplr(fft(E));
mod_new_e=new_e(1:1024);

y=linspace(1,256,length(mod_new_e));
abs_mod_new_e=(abs(mod_new_e)).^2;
norm_abs_mod_new_e=abs_mod_new_e/max(abs_mod_new_e);


ax_10=[min(y),max(y),min(norm_abs_mod_new_e), ...
     max(norm_abs_mod_new_e)];axis(ax_10),
plot(y,norm_abs_mod_new_e),grid,
title(' Detected Intensity in Correlation Plane'),
xlabel(' x '),ylabel(' |F{F{encoded g(x)}}|^2 ')
meta homey5
axis;
```

COSINE.M SOURCE CODE

```
function [V,k] = cosine(o,g,N)
%%%%                                                    March 1993
%%%%
%%%%
%%%%        This program will calculate a cosine signal for use in the
%%%%        actual.m and ideal.m imaging simulation programs.
%%%%

k=linspace(1,25.5,1024);
V=o + g*cos(k);
```

CHIRP.M SOURCE CODE

```
function [V,k] = chirp(o,g,N)
%%%%                                                    March 1993
%%%%
%%%%
%%%%        This program will calculate a chirp signal for use in the
%%%%        actual.m and ideal.m imaging simulation programs.
%%%%


fo=.2;
fd=.5;

k=linspace(0,255,1024);

V=o+g*(sin(k*(fo+fd/2)-(fd*(N-1)/(4*pi)).* sin(2*pi*k/(N-1))));
```

LIST OF REFERENCES

1. Juday, R.D., "Optical Correlation," Johnson Space Center Tracking and Communications Division Annual Summary, 1991.

2. Fielding, K.H., Horner, J.L., and Makekau, C.K., "Modified Two-focal-length Optical Correlator," *Applied Optics*, vol. 29, no. 29, pp. 4332-4333, (1990).

3. Kumar, B.V.K. Vijaya, "A Tutorial Review of Partial-Information Filter Designs for Optical Correlator," *Asia-Pacific Engineering Journal (Part A)*, vol. 2, no. 2, pp 203-215, (1992).

4. Cotariu, S.S., Monroe, S.E., and Knopp, J., "A Live Input, Live Filter, Liquid Crystal Correlator," presented at SPIE's OE/Aerospace Sensing Symposium, Paper no. 1704-29, (April 1992).

5. Juday, R.D., "Optimal Realizable Filters and the Minimum Euclidean Distance Principle", *Applied Optics*, vol. 32, no. 26, pp. 5100-5111, (1993) .

6. Juday, R.D., "Correlation with a Spatial Light Modulator Having Phase and Amplitude Cross Coupling", *Applied Optics*, vol. 28, no. 22, (1989).

7. Kirsch, J.C., Gregory, D.A., Thie, M.W., and Jones, B.K., "Modulation Characteristics of the Epson Liquid Crystal Television", *Optical Engineering*, vol. 31, no. 5, (May 1992).

8. Monroe, S.E., "An Optical Correlator for Six Degrees-of-freedom Tracking," Lockheed Engineering and Sciences Company, (August 1991).

9. Soutar, C., Monroe, S.E., and Knopp, J., "Measurement of the Complex Transmittance of the Epson Liquid Crystal Television," *Optical Engineering*, vol. 33, no. 4, pp. 1061-1068, (1994).

10. Goodman, J.W., *Introduction to Fourier Optics*, McGraw-Hill, New York, 1968.

11. MATLAB for MS-DOS Personal Computers, User's Guide, The MathWorks, Inc., Natick, MA (1990).

12. SPYGLASS TRANSFORM, Version 2.1 Update Manual, Spyglass, Inc., Champaign, IL (1992).

INITIAL DISTRIBUTION LIST

No. Copies

1. Defense Technical Information Center   2
   8725 John J. Kingman Rd., STE 0944
   Ft. Belvoir, VA 22060-6218

2. Dudley Knox Library   2
   Naval Postgraduate School
   411 Dyer Rd.
   Monterey CA 93943-5101

3. Chairman, Code EC   1
   Department of Electrical and Computer Engineering
   Naval Postgraduate School
   833 Dyer Rd., Room 437
   Monterey, California 93943-5121

4. Professor John P. Powers, Code EC/Po   3
   Department of Electrical and Computer Engineering
   Naval Postgraduate School
   833 Dyer Rd., Room 437
   Monterey, California 93943-5121

5. Professor Ron J. Pieper, Code EC/Pr   1
   Department of Electrical and Computer Engineering
   Naval Postgraduate School
   833 Dyer Rd., Room 437
   Monterey, California 93943-5121

6. MAJ Scot C. Miller, USA   2
   AMC STCEUR
   CMR 467, Box 5503
   APO AE 09096